Reprinted from

PHYSICS OF THE EARTH AND PLANETARY INTERIORS

Physics of the Earth and Planetary Interiors 86 (1994) 117–146

Can the differential sensitivity of body wave, mantle wave, and normal mode data resolve the trade-off between transition zone structure and boundary topography?

Eugene M. Lavely *, Arthur Rodgers, Michael H. Ritzwoller

Department of Physics and Cooperative Institute for Research in the Environmental Sciences, University of Colorado, Campus Box 583, Boulder, CO 80309-0583, USA

Received 17 November; accepted 18 March 1994

ELSEVIER

PHYSICS OF THE EARTH AND PLANETARY INTERIORS

Scope of the Journal

Physics of the Earth and Planetary Interiors will be devoted to the application of chemistry and physics to studies of the Earth's crust, mantle and core and to the interiors of the planets. It is hoped that it will attract papers of high originality and, with an international coverage, contribute to the sound development of this well-established field of the Earth and Space Sciences. Types of contributions to be published are: (1) research papers; (2) reviews; (3) short communications, preferably in the *Letter Section* (see Note to Contributors on the back inside cover); (4) discussions; (5) book reviews; and (6) announcements.

Publication Information

Physics of the Earth and Planetary Interiors (ISSN 0031-9201). For 1994 volumes 81–86 are scheduled for publication.

Subscription prices are available upon request from the Publisher. Subscriptions are accepted on a prepaid basis only and are entered on a calendar year basis. Issues are sent by surface mail except to the following countries where air delivery via SAL mail is ensured: Argentina, Australia, Brazil, Canada, Hong Kong, India, Israel, Japan, Malaysia, Mexico, New Zealand, Pakistan, P.R. China, Singapore, South Africa, South Korea, Taiwan, Thailand, USA. For all other countries airmail rates are available upon request.

Claims for missing issues must be made within six months of our publication (mailing) date.

Please address all your requests regarding orders and subscription queries to: Elsevier Science B.V., Journal Department, P.O. Box 211, 1000 AE Amsterdam, Netherlands, tel. 31-20-5803642, fax 31-20-5803598.

For further information, or a free sample copy of this or any other Elsevier Science journal, readers in the USA and Canada can contact the following address: Elsevier Science Inc., Journal Information Center, 655 Avenue of the Americas, New York, NY 10010, USA, tel. (212) 633-3750, fax (212) 633-3764.

All back volumes, except Vols. 5 and 14 are available. Price per volume: Dfl. 321.00 (approx. US$183.40), inclusive of postage, packing and handling. Orders and information requests should be addressed to Elsevier Science B.V., Special Services Department, P.O. Box 211, 1000 AE Amsterdam, Netherlands. *All back volumes are available on microfilm.* Orders and information requests concerning back volumes on microfilm should be addressed exclusively to: Elsevier Science S.A., P.O. Box 851, 1001 Lausanne, Switzerland.

US mailing notice — *Physics of the Earth and Planetary Interiors* (ISSN 0031-9201) is published monthly by Elsevier Science B.V., (Molenwerf 1, Postbus 211, 1000 AE Amsterdam). Annual subscription price in the USA US$1317.00 (valid in North, Central and South America only), including air speed delivery. Second class postage rate paid at Jamaica, NY 11431.
USA POSTMASTERS: Send address changes to *Physics of the Earth and Planetary Interiors* Publications Expediting, Inc., 200 Meacham Avenue, Elmont, NY 11003.
Airfreight and mailing in the USA by Publications Expediting.

ELSEVIER

Physics of the Earth and Planetary Interiors 86 (1994) 117–146

PHYSICS OF THE EARTH AND PLANETARY INTERIORS

Can the differential sensitivity of body wave, mantle wave, and normal mode data resolve the trade-off between transition zone structure and boundary topography?

Eugene M. Lavely *, Arthur Rodgers, Michael H. Ritzwoller

Department of Physics and Cooperative Institute for Research in the Environmental Sciences, University of Colorado, Campus Box 583, Boulder, CO 80309-0583, USA

Received 17 November; accepted 18 March 1994

Abstract

Large-scale seismic models of the three-dimensional (3D) variations in elastic properties will be biased by topography on mantle boundaries to the extent that volumetric and topographic structures produce similar effects in the data. To date, seismic inversions for global-scale 3D elastic models of the mantle have largely ignored the effect that topography on the major mantle discontinuities would have on estimating these models. In this paper we address three questions: (1) to what extent does unmodeled structure on the 410 and 660 km boundaries bias volumetric structure in inversions based on normal mode–mantle wave structure coefficients, absolute S-wave travel times, and differential SS–S travel times? (2) Can the differences in the sensitivity of S waves, SS–S phase pairs, and normal mode–mantle wave data be exploited to estimate transition zone volumetric models that are relatively unbiased by topographic structure? (3) Have current volumetric models resolved the trade-off that exists between volumetric and topographic structures?

To address question (1), synthetic experiments were performed which show that volumetric models inferred from normal mode–mantle wave data can be biased by an average value of 20–25% in r.m.s. amplitude in the transition zone relative to current aspherical Earth models, depending on the model parametrization employed. The average transition zone volumetric bias of models inverted from absolute travel times from both transition zone and lower-mantle bottoming S rays that are imprinted with the same topographic signatures is reduced by at least by a factor of five relative to models inverted from normal mode–mantle wave data alone. A reduction in bias by a factor of about four is obtained using SS–S phase pairs in which the SS legs bottom in both the transition zone and lower mantle. The use of lower-mantle bottoming S rays or SS–S phase pairs with the SS legs bottoming in the lower mantle reduces the bias only by an average factor of about two to three relative to the normal mode–mantle wave inversion. These estimates of bias reduction can vary with the type of damping or smoothness constraints that are applied in the inversion. With respect to question (2), these results suggest that, in principle, absolute S-wave travel time data can be used to desensitize volumetric inversions to the bias caused by topography on the transition zone boundaries. In practice, however, near-source structure that contaminates S-wave travel times would diminish this

* Corresponding author. Telephone: 303-492-4471. Fax: 303-492-7935. email: lavely@lemond.colorado.edu.

SSDI 0031-9201(94)05065-6

capability. The use of SS–S differential times for SS waves which bottom in the transition zone and mantle waves sensitive to transition zone structure but insensitive to the 660 km boundary, should be the most effective means of overcoming the trade-off. To address question (3), we adopt the criterion that the combination of an unbiased volumetric model with an accurate topographic model should provide a better fit to normal mode structure coefficients than the volumetric model alone. The boundary model Topo660a when added to the volumetric model S12_WM13 fits the normal mode structure coefficients significantly better than the volumetric model alone. However, more recent models of 410 and 660 km boundary topography degrade the fit of the volumetric models S12_WM13 and SH.10c.17 to the normal mode structure coefficients, suggesting that there is not yet a conclusive answer to this question.

1. Introduction

A well-specified global seismic model would comprise, in addition to long-wavelength aspherical variations in the isotropic seismic velocities and density, regional wavelength variations in these isotropic parameters, topography on structural boundaries, and some representation of aspherical variations in anelasticity and anisotropy. Current three-dimensional (3D) global seismic models are not yet so complete and, therefore, inversions for seismic models are always underspecified. The problem is that underspecified estimators are invariably biased. In this paper, we continue the investigations started by Ritzwoller and Lavely (1994a) (hereafter R&L) and Rodgers and Wahr (1994) (hereafter R&W) which attempted to estimate the bias in isotropic elastic global models caused by ignoring topography on discontinuities in the interior of the mantle.

Current global 3D seismic models (e.g. Dziewonski, 1984; Woodhouse and Dziewonski, 1984; Tanimoto, 1990; Inoue et al., 1990; Masters et al., 1992; Su et al., 1994) have been inferred independently from estimates of topography on mantle discontinuities (e.g. Revenaugh and Jordan, 1989, 1991a,b; Shearer, 1990, 1991a,b, 1993; Neele and Snieder, 1992; Shearer and Masters, 1992; Vidale and Benz, 1992; Benz and Vidale, 1993; Wicks and Richards, 1993). There are studies that have experimented with the simultaneous estimation of volumetric and boundary models (e.g. Ritzwoller et al., 1988; Smith and Masters, 1989a; Woodward and Masters, 1991a; Li et al., 1991), but these researchers have downplayed the inferred boundary models either as a result of the formal trade-off between volumetric and boundary structures for the normal mode data or because only a marginal variance reduction was achieved for the body wave data when topography on mantle boundaries was included. In the studies of R&L and R&W, topographic models on internal mantle discontinuities were used to construct synthetic surface and mantle wave structure coefficients (R&L) and S-wave travel time residuals (R&W). These synthetic data were then inverted for aspherical volumetric structure (δv_s) in the mantle to estimate the bias of volumetric structures caused by mantle topography. The two synthetic experiments displayed qualitatively similar results: topographic structure biases volumetric structure dominantly in the vicinity of the boundaries and the geographical distribution of the biased structure is strongly correlated with the geographical distribution of the input topographic models. The synthetic experiments of R&L and R&W, however, differed appreciably quantitatively, as the r.m.s. amplitude of the biased volumetric model is a strong function of the types of data employed. The amplitude of the bias is a somewhat weaker function of model parametrization and the method of inversion.

Using the 660 km boundary model of Shearer and Masters (1992), ad hoc but realistic models of topography on the 220 and 410 km boundaries, synthetic long-period mantle and surface wave data, and a simple six-shell mantle parametrization, R&L found that inferred transition zone and uppermost lower-mantle structure may contain a 25–30% bias relative to the magnitude of aspherical volumetric structure owing to topographic aliasing. For a geodynamically derived 660 km topographic model, using S waves piercing the 660 km discontinuity and a radial model

parametrized with Chebyshev polynomials with a higher resolution than the six-shell basis of R&L, R&W concluded that the level of biasing would be smaller than that estimated using surface and mantle wave data. The amplitude of this bias is a strong function of the radial resolution of the inferred volumetric model.

It is difficult to compare the results of these two studies quantitatively, as different volumetric model parametrizations were used and different input topographic models were employed. However, if we attempt to correct for these differences between the studies of R&L and R&W, topographic aliasing into volumetric structure in the transition zone from S-wave absolute travel time data with the S legs bottoming in and below the transition zone appears to be about 20% or less of the surface–mantle wave bias, or only about 5% in r.m.s. of the magnitude of aspherical volumetric structure in this region.

It is clear that topography on the transition zone discontinuities will be biased into large-scale volumetric models, but the magnitude and sign of the bias will be a function of the relative weighting of the surface–mantle wave data and the body wave data used in each inversion, and will also be dependent on model parametrization and the technique of inversion. The current paper aims to characterize more clearly and to quantify the respective volumetric biasing produced by transition zone boundary topography when normal mode–mantle wave and body wave data are employed, and addresses whether a method to exploit the characteristics of these diverse data could be designed to infer volumetric transition zone structure accurately given the likely topography on the boundaries of the region.

We attempt to answer three questions: (1) if normal mode–mantle wave, S-wave absolute travel time, and SS–S differential travel time synthetic experiments are performed such that input topographic models are identical and the biased volumetric models are parametrized identically, what is the relative level of r.m.s. bias for the three different data types? (2) Can these differences be exploited to estimate relatively unbiased volumetric models, while retaining the information from both the normal mode–mantle wave and body wave data sets? (3) What is the relationship between Shearer's models of transition zone boundary topography and the volumetric models in that region? Have current global models of volumetric structure in the transition zone already resolved the trade-off?

There are a number of problems of geophysical significance that demand the resolution of the trade-off between boundary topography and volumetric structure. For example, the question of whether mantle flow is stratified by changes in the bulk chemistry or phase across the 660 km boundary hinges on the accurate determination of volumetric structure across the boundary and of boundary topography itself; e.g. the use of radial correlation functions of seismic volumetric structure as described by Jordan et al. (1993) to discriminate between competing models of convection. Another example is the need for volumetric models that have resolved the trade-off so that seismic estimation of boundary models that rely on ray tracing corrections, as used by Shearer (1993), would be minimally biased. Finally, accurate knowledge of the 410 and 660 km boundaries as well as the volumetric structure in their vicinity is crucial for seismic determination of the fate of slabs, Clapeyron slopes, viscosity contrasts, and convective flow patterns.

In Section 2, we discuss the nature of the synthetic experiments carried out in this paper. Section 3 presents the results from the synthetic experiments. Section 4 is a discussion of the fit of combined volumetric–topographic models to normal mode data. Section 5 is a discussion of the implications of these experiments.

2. Input models and synthetic data construction

2.1. Volumetric and topographic models

There are, in general, two types of elastic, isotropic aspherical structures in the interior of the Earth. The first is lateral heterogeneity in the elastic moduli ($\delta\kappa$, $\delta\mu$) and density ($\delta\rho$) (or equivalently the seismic velocities (δv_p, δv_s) and density). These asphericities are referred to generically as volumetric structures. The second

type of aspherical structure is topography on first-order boundaries in the interior of the Earth (h_d on boundary d), where a first-order boundary is the location of a discrete jump of the seismic parameters across a given radius.

There now exist several global-scale 3D elastic models of the mantle, including the upper-mantle δv_s models M84A and M84C (Woodhouse and Dziewonski, 1984), the lower-mantle δv_p model LO2.56 (Dziewonski, 1984), and the whole-mantle δv_s models MDLSH (Tanimoto, 1990), SH.10c.17 (Masters et al., 1992), SH8WM13 (Woodward et al., 1993), and S12_WM13 (Su et al., 1994). All of these models use the spherical model PREM (Preliminary Reference Earth Model; Dziewonski and Anderson, 1981) as a reference to which aspherical perturbations are added. A variety of seismic body wave, mantle wave, and normal mode data have been used in the construction of these models. (Mantle waves are very long period (more than 100 s) Rayleigh and Love waves.) These models have traditionally been constructed relative to an a priori reference crustal model, albeit different crustal models, but no correction has been applied to any of the models for the effects of topography on boundaries outside of the crust. A recent review of and comparison among these 3D mantle models has been presented by Ritzwoller and Lavely (1994b). A number of other studies have contributed to the developing understanding of the 3D seismic volumetric structure of the Earth, including (to mention but a few of the most recent studies) Nishimura and Forsyth (1989), Smith and Masters (1989a), Montagner and Tanimoto (1990, 1991), Inoue et al. (1990), Roult et al. (1990), Woodward and Masters (1991a,b), Zhang and Tanimoto (1993) and Pulliam et al. (1993). A review of some of these and other tomographic studies has been presented by Romanowicz (1991).

Models of topography on boundaries in the interior of the mantle have been constructed in two very different ways:

(1) the earliest global-scale models of topography on mantle discontinuities were derived from the volumetric seismic models by geodynamical computations. Tomographic images were converted to density anomalies and, together with excess density in the slabs, were entered as body forces into the equations of motion for buoyantly driven viscous flows, thus predicting boundary topography and certain surface observables, such as the geoid, plate motions, and surface topography (e.g. Hager, 1984; Hager et al., 1985; Forte and Peltier, 1989, 1991; Hager and Clayton, 1989; Hager and Richards, 1989; Dehant and Wahr, 1991; Forte et al., 1993). Reviews of some of these studies have been presented by Olson et al. (1990) and Dziewonski et al. (1993).

(2) Seismologists have also studied reflected and transmitted waves that impinge on the core–mantle boundary (CMB) (e.g. Creager and Jordan, 1986; Gudmunsson et al., 1986; Morelli and Dziewonski, 1987; Rodgers and Wahr, 1993) and underside and topside reflections and phase-conversions off the transition zone and upper-mantle discontinuities (e.g. Paulssen, 1988; Revenaugh and Jordan, 1989, 1991a,b; Richards and Wicks, 1990; Shearer, 1991a,b, 1993; Neele and Snieder, 1992; Shearer and Masters, 1992; Vidale and Benz, 1992; Benz and Vidale, 1993; Wicks and Richards, 1993) in attempts to infer the nature of and topography on mantle discontinuities. The only global seismically inferred models of topography on the transition zone boundaries at 410 and 660 km depth are those of Shearer and Masters (1992) and Shearer (1993). These models will be discussed further in Section 2.2. Like the geodynamically derived topographic models, a number of the seismological models of boundary topography have been constructed relative to input 3D volumetric models which have been used to 'correct' the data for volumetric effects prior to inversion for boundary topography (e.g. Shearer, 1993).

Volumetric and topographic structures have been represented in a number of ways. Radial variations in volumetric structures have been represented either in terms of continuous basis functions (Legendre or Chebyshev functions) or discrete, piecewise constant spherical shells. Lateral volumetric and topographic variations have been usually represented with spherical harmonics. Here, we reparametrize all models in terms of fully normalized complex spherical harmonics:

$$\delta m(r, \theta, \phi) = \sum_{s,t} \delta m_s^t(r) Y_s^t(\theta, \phi) \quad (1)$$

$$h_d(\theta, \phi) = \sum_{s,t} h_{ds}^t Y_s^t(\theta, \phi) \quad (2)$$

where $\delta m(r, \theta, \phi)$ represents a volumetric perturbation relative to an elliptical reference state (e.g. δv_s, δv_p, $\delta\kappa$, $\delta\mu$, $\delta\rho$) and h_d represents topography on the dth boundary, again in excess of ellipticity. The spherical harmonic indices are referred to as the degree s and order t of aspherical structure.

2.2. Global models of transition zone topography

Currently, there exist two published studies that resulted in global models of topography on the 660 km discontinuity (Shearer and Masters, 1992; Shearer, 1993) and one study that produced models of topography on the 410 km discontinuity (Shearer, 1993). Both of these studies used stacking methods to enhance underside reflected precursors to SS called SdS, to model transition zone boundary topography with the differential SS–SdS travel times. These studies differed in the methods employed to 'correct' the data for the effects of volumetric structure and surface topography. Shearer and Masters (1992) used observed SS–S differential travel times to desensitize the observed SS measurements to upper-mantle structure, whereas Shearer (1993) utilized the seismic volumetric models SH.10c.17 and SH8WM13, surface topography estimates, and an ad hoc crustal model to correct the SS travel times explicitly. The former study yielded the model Topo660a, whereas the later study produced the models Topo410b and Topo410c as well as Topo660b and Topo660c. The suffices 'b' and 'c' in the model names refer to the volumetric models used to correct the SS–SdS observations; 'b' refers to SH.10c.17 and 'c' refers to SH8WM13. Figs. 1(a) and 1(b) display these boundary models. The geographical correlations between the models are listed in Table 1 as a function of degree s. The correlation value that corresponds to the 95% confidence level is shown in the right-most column of the table.

2.3. Synthetic normal mode and mantle-wave data

The effect of both volumetric structure and boundary topography on the Earth's normal modes is contained in the components $H_{k'k}^{m'm}$ of the splitting matrix $\boldsymbol{H}_{k'k}$ (Woodhouse and Dahlen, 1978; Woodhouse, 1980). Here $k = (n, l)$ is the multiplet identifier. Ignoring contributions from the Earth's rotation, ellipticity of figure, and the interaction between multiplets ($k = k'$), the splitting matrix can be written

$$H_{kk}^{m'm} = \sum_{s} \sum_{t=-s}^{s} \gamma_s^{m'm}{}_k c_s^t \quad (3)$$

where $\gamma_s^{m'm}$ depends on Wigner 3-j symbols and t is constrained to the value $m' - m$ by the selection rules that govern $\gamma_s^{m'm}$. The normal mode structure (or interaction) coefficients are denoted by ${}_k c_s^t$ and are simply related to aspherical volumetric and boundary structures:

$${}_k c_s^t = \int_0^a {}_k K_s(r) \delta m_s^t(r)\, \mathrm{d}r + \sum_d {}_k D_{ds} h_{ds}^t \quad (4)$$

$$= {}_k \tilde{c}_s^t + {}_k \hat{c}_s^t \quad (5)$$

where ${}_k \tilde{c}_s^t$ is the structure coefficient computed from volumetric structure alone and ${}_k \hat{c}_s^t$ is the structure coefficient computed from boundary structure alone. Here, $K_s(r)$ is the volumetric kernel and ${}_k D_{ds}$ is the boundary kernel for boundary d, both given by Woodhouse and Dahlen (1978), and $\delta m_s^t(r)$ and h_{ds}^t represent the spherical harmonic coefficients for the volumetric structure (e.g. δv_s, δv_p, $\delta\rho$) and boundary topography, respectively, given by Eq. (1). The fully normalized complex spherical harmonics $Y_s^t(\theta, \phi)$ are normalized according to the convention of Edmonds (1960). Eq. (4) is valid only for even-degree s structure coefficients. Odd-degree structure coefficients are defined in a similar way, but they are more complicated as their volumetric and boundary kernels depend on the radial eigenfunctions of two multiplets. A full discussion of this has been given by Woodhouse (1980). The structure coefficients for each multiplet form the splitting matrix and, therefore, determine the frequencies and shapes of the seismic oscillations. Their use as expansion coefficients in a spherical

harmonic expansion (with a suitable multiplicative factor) results in a splitting function or phase velocity map (e.g. Giardini et al., 1988). The use of fully normalized spherical harmonics implies that as each scalar representation considered is real, the structure coefficients satisfy the relationship $c_s^{-t} = (-1)^t c_s^{t*}$, where * denotes the complex conjugate. Thus, a degree s scalar field is fully specified by the azimuthal orders $0 \leqslant t \leqslant s$. The real and imaginary components of c_s^t are denoted, respectively, by $\mathrm{Re}c_s^t$ and $\mathrm{Im}c_s^t$.

The boundary kernels ${}_kD_{ds}$ contained in the definition of the normal mode structure coefficients (Eq. (4)) define the sensitivity of a multiplet to topography on a given boundary. Fig. 2 shows the normalized boundary kernels for topography on the 660 km (solid line) and 410 km (dotted line) boundaries for long-period multiplets along the fundamental mode branch. Modal sensitivity to the 660 km boundary is fairly band-restricted and peaks near ${}_0S_{23}$. Sensitivity to the 410 km boundary is broader in frequency and peaks near ${}_0S_{37}$.

2.4. Synthetic body wave data

For reasons that will become apparent in Section 3, we consider four body-wave data sets:

(1) the first data set consists of S waves that penetrate the 410 and 660 km discontinuities and

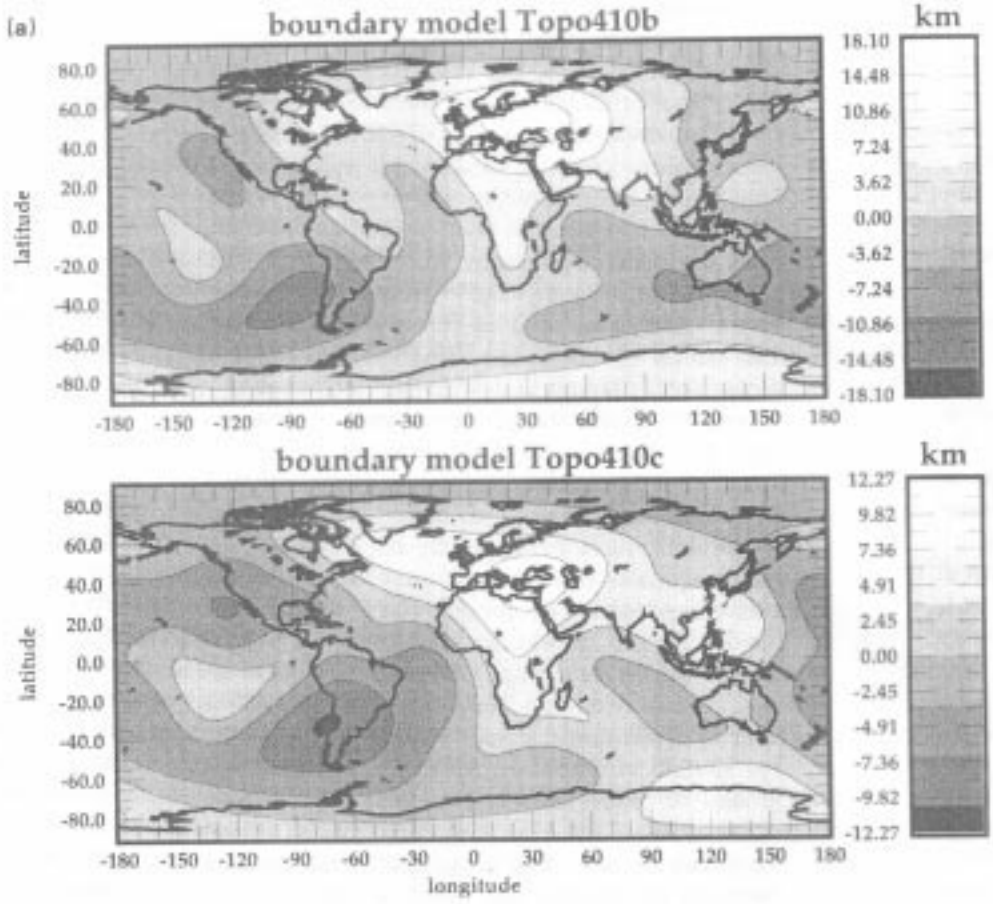

Fig. 1. (a) The models Topo410b and Topo410c of topographic structure on the 410 km boundary from Shearer (1994). (b) The models Topo660a, Topo660b, and Topo660c of topographic structure on the 660 km boundary from Shearer and Masters (1992) and Shearer (1993). Geographic correlations of the models are listed in Table 1 as a function of degree of structure.

bottom in the lower mantle only. These data are sensitive to topographic structure on both the 410 and 660 km discontinuities.

(2) The second data set contains S waves that bottom in the lower mantle, below 660 km depth, and in the transition zone. The S rays that bottom

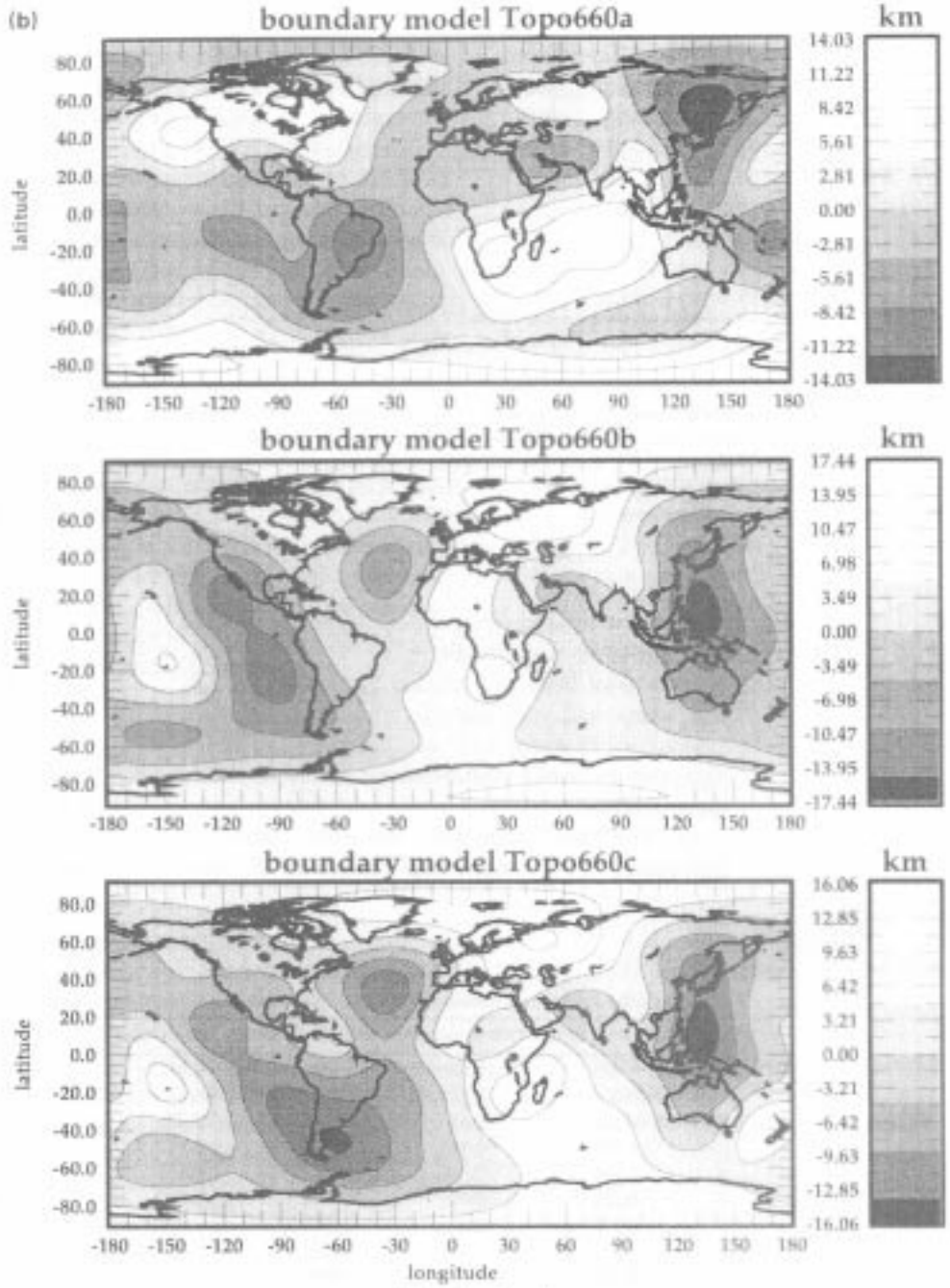

Fig. 1 (continued).

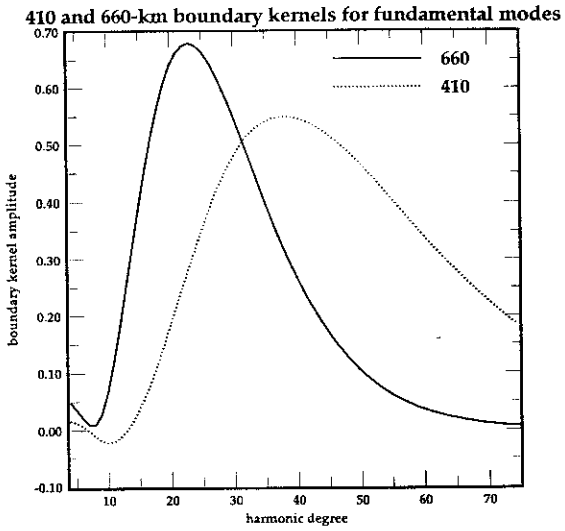

Fig. 2. Normalized sensitivity of fundamental normal modes–mantle waves to topography on the 410 km boundary (dotted line) and 660 km boundary (solid line); i.e. the boundary kernels, ${}_kD_{ds}$, from Eq. (4). Peak sensitivities to the 410 and 660 km boundaries are in the ranges $30 \leqslant l \leqslant 50$ and $20 \leqslant l \leqslant 35$, respectively.

in the transition zone are insensitive to 660 km topography in the ray-theoretic approximation. The paths of both sets of rays are shown in Fig. 3(a). Rays with ray parameters associated with S-wave triplications are not included in these data sets to avoid complications in interpreting these arrivals.

(3) The third body-wave data set comprises differential travel times computed for SS–S phase pairs, and the ray parameters are chosen such that the SS legs bottom in the lower mantle only. The ray paths of the SS–S phase pairs that correspond to the minimum and maximum ranges of the S waves of this data set are shown in Fig. 3(b).

(4) The fourth body-wave data set consists of SS–S phase pairs with SS legs bottoming in both the transition zone and the lower mantle.

The synthetic data sets are constructed to have uniform geographical sampling of the transition zone boundaries. This results in the sources and receivers being uniformly distributed around the globe, and eliminates possible biases associated with non-uniform sampling. Consequently, the ability of realistic data distributions to image the transition zone and the surrounding boundaries should be degraded relative to the results presented here.

The relationship between topographic structure and travel times has been derived by Dziewonski and Gilbert (1976) and R&W. The travel time perturbation, δt, for a ray passing through a perturbed boundary d, with topography $h_d(\theta,\phi)$ is given by

$$\delta t = -h_d(\theta, \phi)\left(\frac{\cos i_+}{v_+} - \frac{\cos i_-}{v_-}\right) \tag{6}$$

where i is the incident angle, v is the ray velocity and the plus and minus signs correspond respectively to the values directly above and below the boundary. These formulae are used to compute

Table 1
Geographical correlation between the topographic models Topo410b, Topo410c, Topo660a, Topo660b, and Topo660c

s	410b vs. 660b	410c vs. 660c	410b vs. 410c	660b vs. 660c	660a vs. 660b	660a vs. 660c	95% confidence
1	0.425	0.838	0.939	0.668	0.423	0.258	0.95
2	0.874	0.759	0.845	0.888	0.590	0.727	0.81
3	−0.202	−0.61	0.833	0.771	−0.382	−0.626	0.71
4	0.768	0.114	0.750	0.893	0.364	0.502	0.63
5	0.848	0.408	0.844	0.875	0.881	0.622	0.58
6	−0.356	−0.404	0.846	0.853	0.298	0.364	0.53
7	0.575	0.495	0.890	0.856	0.457	0.635	0.50
8	0.037	0.151	0.857	0.744	0.502	0.785	0.48
1–8	0.422	0.298	0.880	0.826	0.414	0.403	n.a. [a]

[a] not applicable.

the travel time effects of Shearer's topographic models Topo410b and Topo660b on each ray.

The transition zone bottoming subset of S waves is composed of 9898 rays with epicentral distances ranging from 17 to 30°. The lower-mantle bottoming subset totals 9479 rays with epicentral distances ranging from 19 to 100°. The first SS–S data set consists of 9505 phase pairs with SS legs bottoming in the lower mantle only with epicentral distances ranging from 40 to 100°. In this range, SS and S rays penetrate both the 410 and 660 km discontinuities. The second SS–S data set includes the first SS–S data set and an additional 9741 phase pairs in which the SS legs bottom in the transition zone. The epicentral distances of these additional phase pairs range from 35 to 61°.

The travel time perturbation produced by each boundary depends on the angle of incidence of the ray at the boundary. Fig. 4(a) shows the travel time perturbations of vertically incident S waves computed for the input topographic models Topo410b (top panel) and Topo660b (bottom panel). As vertically incident rays are affected least by topography, this figure represents the minimum effect of topographic structure on ray travel times. Travel time perturbations for non-vertically incident rays can be inferred from Figs. 4(a) and 4(b) in the following way. Fig. 4(b) displays the travel time perturbation related to 18 km of topography on the 410 and 660 km discontinuities as a function of both incidence angle (top panel) and ray parameter (bottom panel) for the rays used in this study. The value of 18 km was chosen as the maximum amplitude perturbation of Topo660b is about 18 km. The plotted points are multiplicative factors to be applied to the travel time perturbations for the vertically incident rays shown in Fig. 4(a). The notation SLM and STZ denotes, respectively, lower-mantle and transition zone bottoming S rays. The maximum observable travel time perturbation for the lower-mantle bottoming rays is about 0.95 s for the 660 km discontinuity and about 0.20 s for the 410 km discontinuity. The maximum observable travel time perturbation for the transition zone bottoming data (which are sensitive only to 410 km topography) is 0.79 s.

3. Inversions for biased volumetric structure

The basic method employed in the inversions of synthetic data is described in this section. Noise-free, ideally distributed synthetic data are computed from input topographic models and are then inverted for volumetric structure which is then interpreted as the bias caused by topographic structure. The radial variation of volumetric structure is parametrized in two ways: discretely with 12 spherical-shell radial basis functions, and continuously with Chebyshev basis functions expanded to Degree 7. The Chebyshev representation was motivated by Su et al. (1994) and the shell representation follows that of Masters et al. (1992). The shell representation is the same discretization as used by Tanimoto (1990), but with the addition of a layer near the surface. All lateral variations are parametrized with spherical harmonics as in Eqs. (1) and (2).

For the mantle-wave and free oscillations data, noise-free normal mode structure coefficients are computed and are then inverted. The assumption that they are noise-free is equivalent to the assumption that they are estimated with an ideally distributed set of sources and receivers. The S-wave travel time residuals are computed for a set of sources and receivers distributed nearly evenly over the globe and are partitioned into two subsets depending on whether the rays bottom in the lower mantle alone, or bottom in both the transition zone and the lower mantle. The S-wave travel time residuals from each ray set are inverted independently for volumetric structure. Finally, synthetic SS–S differential travel times are inverted for the case in which the SS legs bottom in the lower mantle only, and the case in which the SS legs bottom in and below the transition zone.

The means of matrix damping and regularization will affect the r.m.s. amplitude and sign of the estimated volumetric models, and therefore, care must be taken so that the bias estimates from the various data sets can be meaningfully compared. The means of damping that we employ differs as a function of data set and model parametrization. For example, the Chebyshev based inversions are damped by applying norm

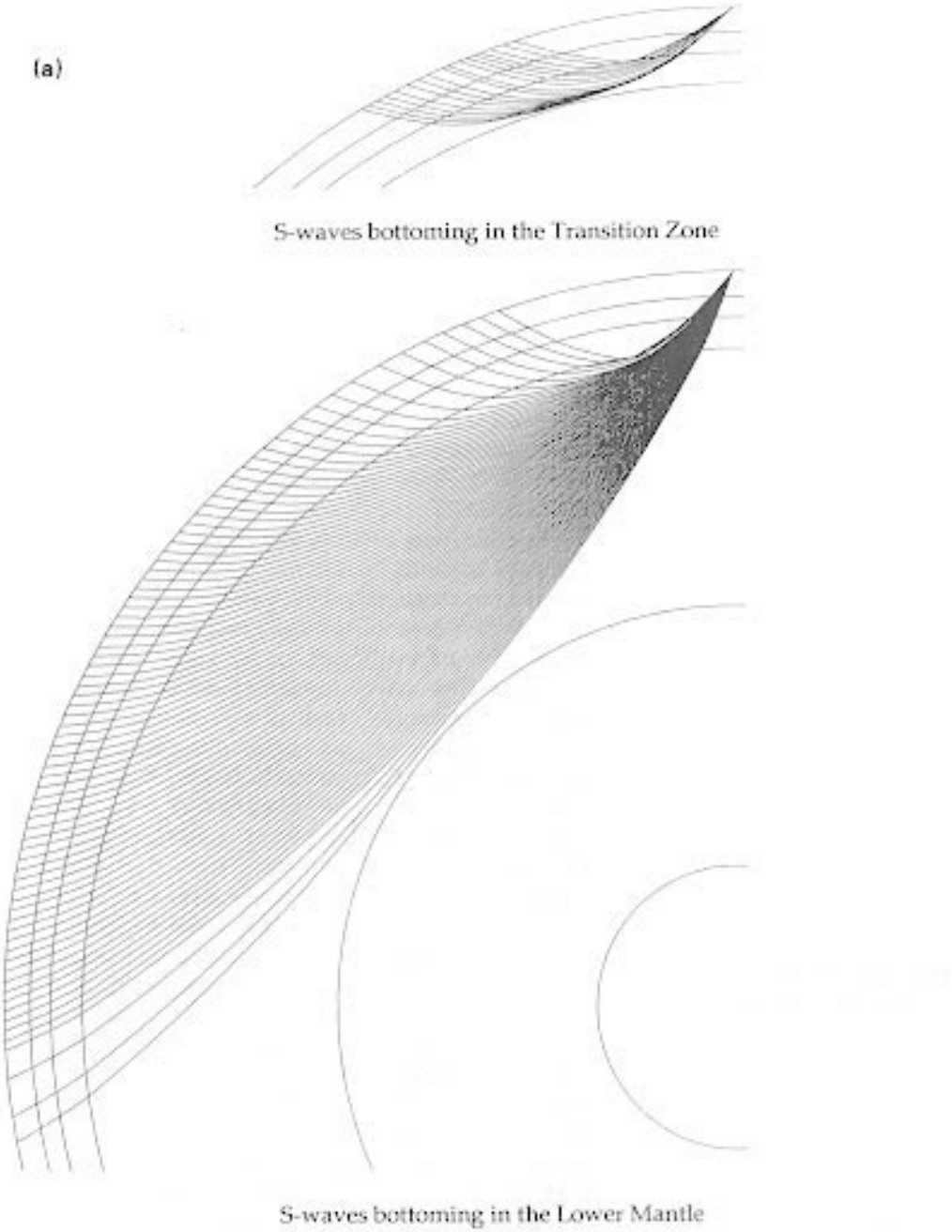

Fig. 3. (a) Body wave sampling plots for S-waves bottoming in the transition zone (top) and in the lower mantle (bottom). (b) Body wave sampling plots showing examples of SS–S phase pairs used in the SS–S inversion experiment in which the SS legs bottom in the lower mantle only. The epicentral distances of the S waves ranged from 40 to 100°.

constraints on the Chebyshev expansion coefficients for which we invert. Also, truncation of the Chebyshev expansions at Degree 7 provides a natural smoothing relative to the Degree 13 Chebyshev expansion used by Su et al. (1994). The shell-based inversions are regularized by

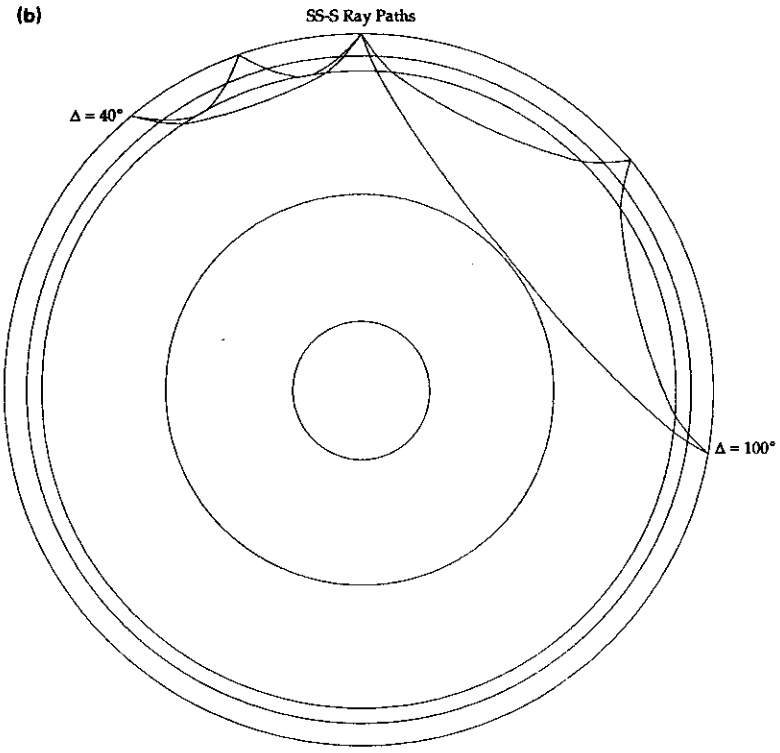

Fig. 3 (continued).

minimizing a roughness or second derivative norm across layers. The weights assigned to the damping or smoothing parameters are chosen so as to reduce data misfit by only a few per cent, but which reduce radial oscillations (a single sign change in the upper mantle is allowed) in the inverted model and large model norms.

3.1. Synthetic normal mode and mantle wave data

The inversion experiments reported in this section were performed with surface wave and mantle wave equivalent multiplets along the fundamental mode branch as well as low-degree multiplets along the lower overtone branches. In particular, the multiplets chosen correspond to the low-degree fundamental and overtone multiplets from the first, second, and fifth branches observed by Ritzwoller et al. (1988) (ignoring the ten anomalously split multiplets which are strongly sensitive to core structure) and those for the mantle–surface wave multiplets ${}_0S_8 - {}_0S_{52}$ observed by Smith and Masters (1989a).

Inversion experiments for three separate synthetic data sets were performed. In the first two experiments synthetic structure coefficients, ${}_k\hat{c}_s^t$ (Eqs. (4) and (5)), were computed using, respectively, the topographic models Topo410b and Topo660b independently, and were inverted for biased volumetric structure. In the third experiment the synthetic data were computed using the combined model Topo410b + Topo660b. It follows from Eq. (4) that inversion for each degree and order of volumetric structure decouples from all other degrees and orders of structure. The normal mode structure coefficients computed are just the self-coupling coefficients, which are only sensitive to the even degrees of structure. Consequently, all bias estimates will be for even degrees alone. The inclusion of odd-degree struc-

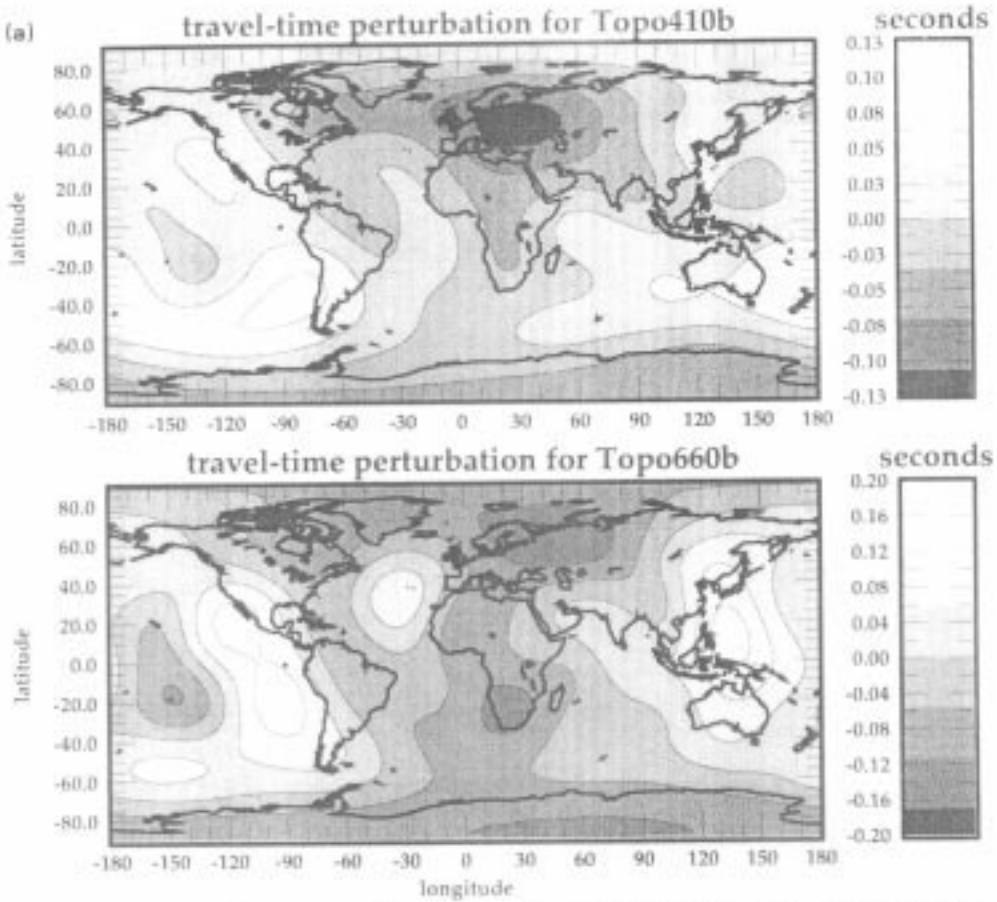

Fig. 4. (a) S-Wave travel time perturbations caused by the topographic models Topo410b and Topo660b mapped to the boundary crossing points for vertically incident S rays. This figure shows the minimum travel time perturbation. Travel time perturbations for non-vertically incident rays can be estimated by applying the multiplicative factors in (b) to the travel time perturbations shown here. (b) Multiplicative factors to be applied to the travel time perturbations shown in (a) to estimate travel time perturbations for S rays that are non-vertically incident upon 18 km of relief on the 410 and 660 km discontinuities. These multiplicative factors are plotted as a function of incident angle (top panel) and ray parameter (bottom panel) in the ranges applicable to the rays bottoming in the lower mantle and transition zone, SLM and STZ, respectively. The notation δT_{670} and δT_{400} denotes the value of the multiplicative factors for the respective boundaries.

ture coefficients would require the adoption of multiplet–multiplet coupling (e.g. Park, 1987), but would not change the conclusions here.

Inversions of the synthetic data sets using the Chebyshev and shell-based model parametrizations yield volumetric models that fit the synthetic structure coefficients nearly perfectly. The nearly 100% variance reductions obtainable in the undamped inversions reflect the nearly exact trade-off between volumetric and topographic structures, which follows as the data are free of noise and the volumetric models are over-parametrized. However, the volumetric models that fit the data optimally are oscillatory with radius. The introduction of smoothness constraints leads to considerably smoother models with minimal sacrifice in data misfit and the biased volumetric models presented for the normal mode–mantle wave data incorporate smoothing. Smoothness constraints were applied to the models parametrized in terms of Chebyshev polynomials by weighting down contributions from polynomials

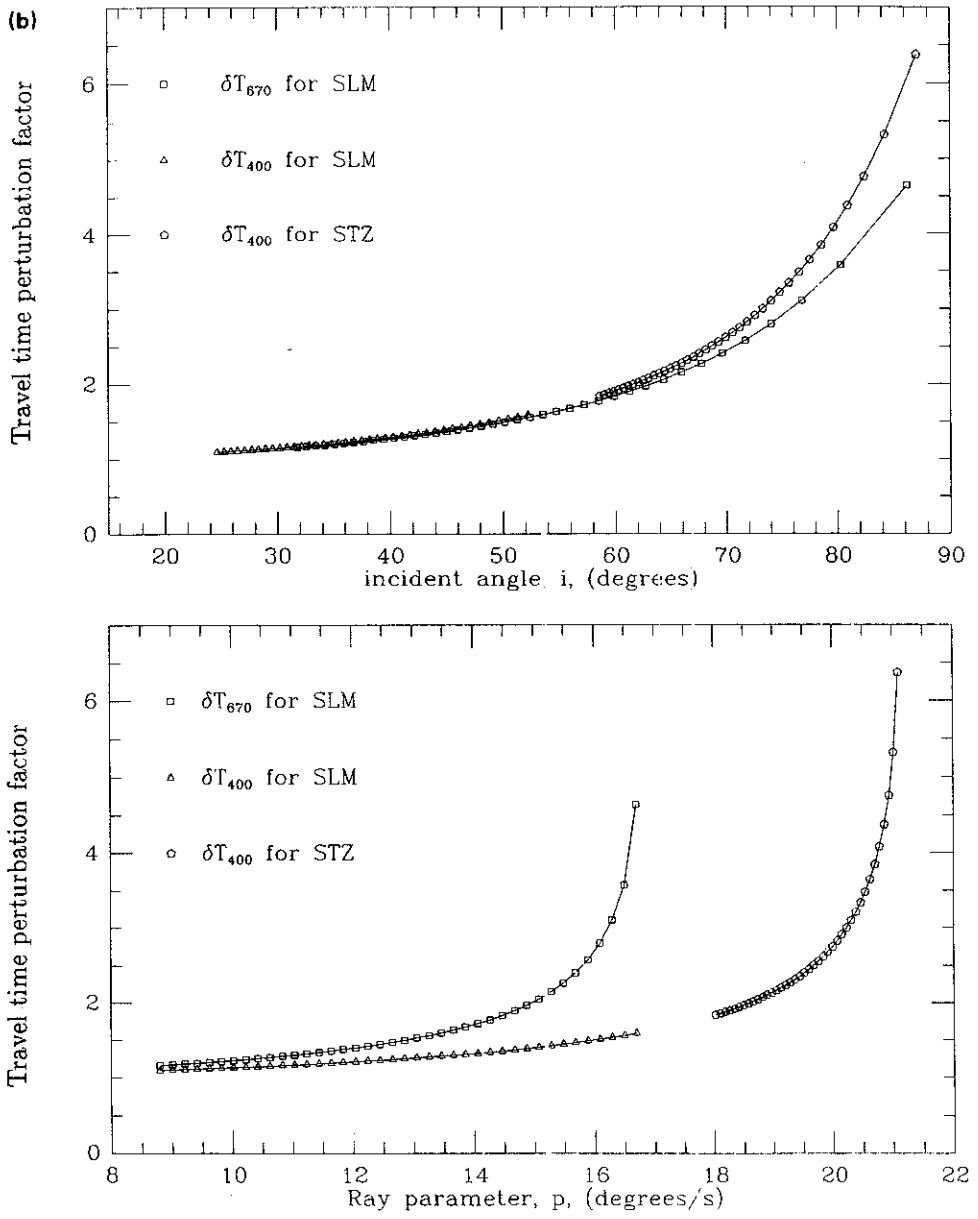

Fig. 4 (continued).

greater than Degree 7, and to the shell-based models by introducing a Lagrange multipler which is multipled by the second derivative of the velocity perturbation across layers. The weights assigned to the smoothness constraints were chosen such that the inversions yielded about 98% variance reductions to the predicted structure coefficients. The addition of these constraints reduced the condition number of the regression matrices by several orders of magnitude to acceptable values (about ten). The resulting volumetric bias models typically vary smoothly across most of the upper mantle and through the top regions of the lower mantle, but tend to oscillate in regions of

rms volumetric bias from Topo410b relative to S12_WM13

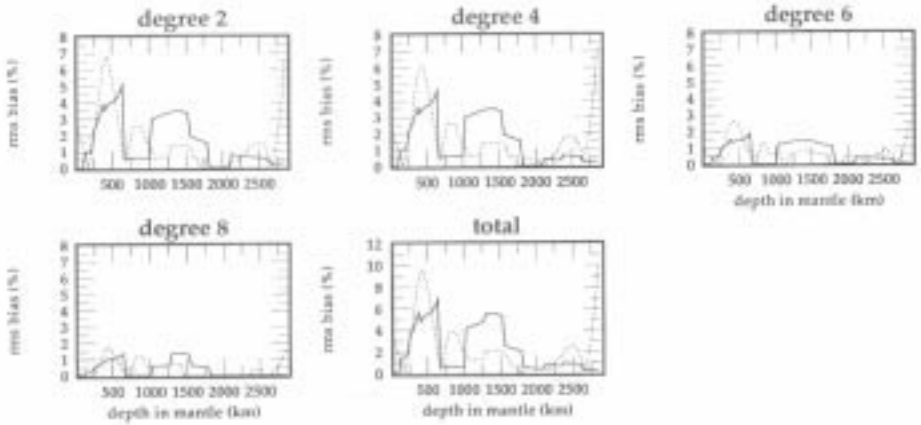

rms volumetric bias from Topo660b relative to S12_WM13

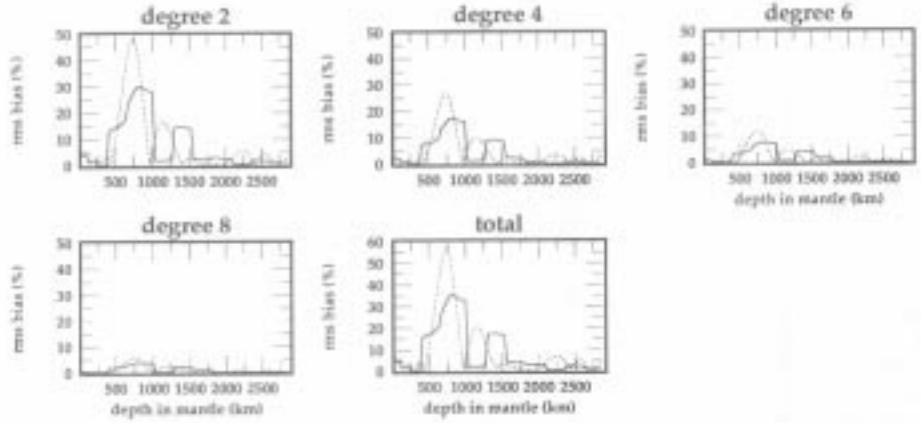

rms volumetric bias from Topo410b+Topo660b relative to S12_WM13

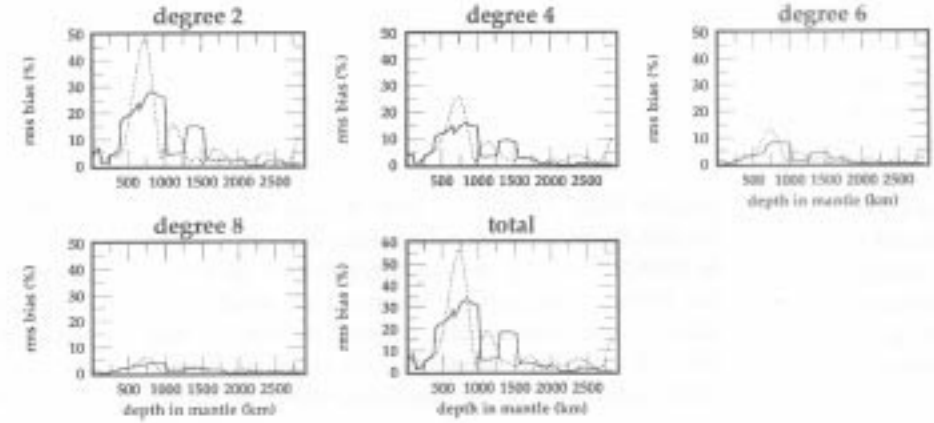

small r.m.s. bias near the top and bottom of the mantle.

Fig. 5(a) displays the r.m.s. of the estimated volumetric bias (per cent shear velocity perturbation relative to the even-degree components of the volumetric model S12_WM13) caused by the topographic model Topo410b as a function of depth for even degrees of structure $2 \leqslant s \leqslant 8$. The bottom right-hand panel displays the contribution to the r.m.s. summed over all degrees of structure. The lower degrees of structure dominate the value of this statistic. The biased volumetric model for the shell (solid line) and Chebyshev (dotted line) parametrizations display broad peaks in the transition zone near the 410 km boundary with average perturbations ranging from about 5% to about 7% relative to S12_WM13. The discrete shell model tends to display broader, lower amplitude (6% maximum) features than the continuous Chebyshev model (9% maximum).The largest amplitude of the continuous model occurs in a narrow radial region near the base of the mantle, whereas the r.m.s. amplitude of the shell-based model is nearly minimized in this region. This tendency of the continuously parametrized model to maximize near the boundaries of the mantle is also seen in the body wave inversion described in Section 3.2, and indicates that inversions with this parametrization should penalize the model norm of the resulting models in these regions. The Chebyshev and shell models fit the synthetic data equally well.

The r.m.s. volumetric bias caused by Topo660b relative to S12_WM13 is shown in Fig. 5(b). The dominant contribution to the total bias is from Degree 2. The volumetric bias is peaked near the 660 km boundary and the average value of the bias in the transition zone is about 15% to about 20% relative to S12_WM13, but peaks at somewhat greater values in the top of the lower mantle. The r.m.s. of the volumetric bias caused by the combined models Topo410b and Topo660b (Fig. 5(c)) is very similar to the bias caused by Topo660b alone, but is spread over a broader region surrounding the transition zone and extends to shallower depths. As Table 1 shows, Topo410b and Topo660b are positively correlated at most degrees and, therefore, their effects constructively interfere. The volumetric bias model inverted from the synthetic data derived from Topo410b and Topo660b is strongly correlated geographically with these models in the vicinity of the respective boundaries.

3.2. Synthetic body wave data

Analogous to the normal mode–mantle wave inversion experiments described in Section 3.1, body wave travel time data were inverted to determine the extent to which unmodeled topographic structure on transition zone boundaries can bias volumetric mantle structure. Four inversion experiments were performed, distinguished by the data used in the inversion:

(1) In the first experiment, travel times for rays that bottom in the lower mantle containing topographic imprints from the boundary models Topo410b and Topo660b were inverted for volumetric structure.

(2) In the second experiment, rays that bottom both in the transition zone (these rays are sensitive only to the topographic model on the 410 km boundary) and in the lower mantle were inverted.

(3) The third experiment utilized SS–S differential travel times at ranges at which both of the phases bottomed in the lower mantle, so that the travel times were sensitive to topographic structure on both the 410 and 660 km discontinuities.

Fig. 5. (a) The r.m.s. of the volumetric bias caused by the topographic model Topo410b, estimated from the inversion of the normal mode–mantle wave data presented as a function of harmonic degree of structure. The volumetric bias has been divided by the r.m.s. of the even-degree components of the reference aspherical volumetric model S12_WM13 at each depth, and the units are in per cent perturbation relative to S12_WM13. The r.m.s. of the volumetric bias model summed over all even degrees is shown at the bottom right. The solid line is the biased volumetric model using the 12 spherical-shell radial basis functions and the dotted line is the model using Chebyshev polynomials to Degree 7 as radial basis functions. (b) Same as (a), but for the topographic model Topo660b. (c) Same as (a) and (b), but for the combined topographic model Topo410b + Topo660b.

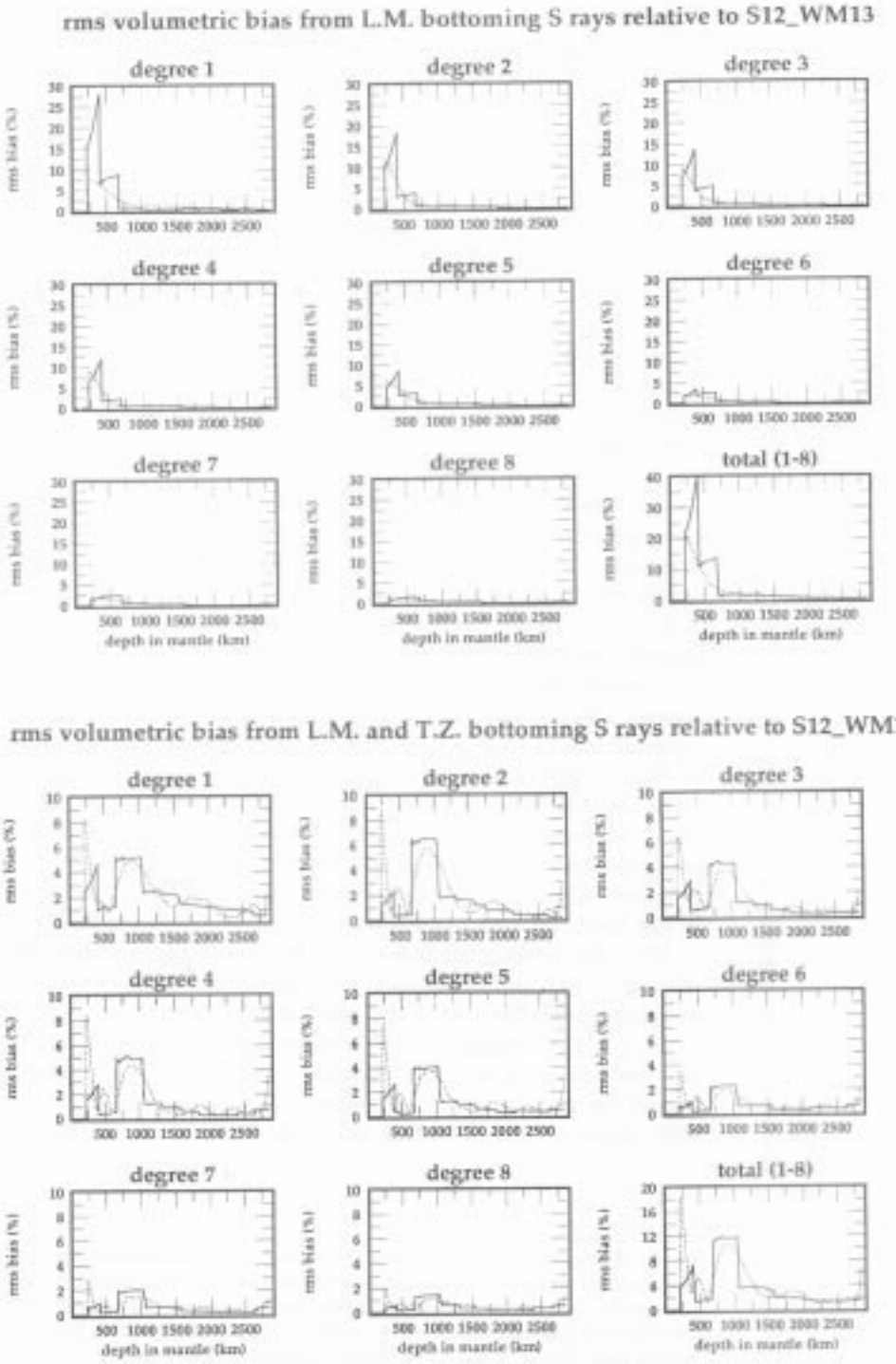

Fig. 6. (a) Similar to Fig. 5(c), but for S waves bottoming in the lower mantle. (b) Similar to (a), but for both S waves bottoming in the lower mantle and the transition zone.

(4) The fourth experiment used SS–S phase pairs chosen such that the SS legs bottomed in both the transition zone and the lower mantle. Unlike the normal mode structure coefficients considered in Section 3.1, body wave travel times are sensitive to both even- and odd-degree structures and inversion results from both types of structures will be presented.

The synthetic body wave data sets used here could not stably constrain structure above 220 km depth and, therefore, the top radial level of the shell and Chebyshev model parametrizations was set to this depth. The inversions based on the low-degree Chebyshev expansions yielded models without undue oscillations, and therefore, the Chebyshev-based inversions were not damped or constrained to be smooth. To make the Chebyshev and shell-based inversions comparable, the shell-based inversions were undamped as well. Thus, the shell-based models typically contain one major oscillation in the upper mantle, not unlike the radial oscillation present in current global models of the upper mantle for numerous degrees and orders. The integrated amplitudes of the Chebyshev and shell-based biased volumetric models are similar.

The models of biased volumetric structure estimated from the four body wave data sets generally provide variance reductions a few per cent below the variance reductions obtained from the inversion of the normal mode–mantle wave data considered in Section 3.1. The variance reductions for the SS–S data sets are generally greater than those for the absolute S-wave data sets. Models inverted from normal mode–mantle wave data or from SS–S data are able to spread structure over a wide radial interval and still fit the data, whereas the absolute S waves have greater localized sensitivity to topography, and thus require parametrizations with similar resolution to fit the data with greater accuracy.

3.2.1. Inversion with absolute S-wave travel times

Fig. 6(a) shows the r.m.s. amplitude (in per cent) of the shear velocity perturbation relative to all degrees of the volumetric mantle model S12_WM13 in the depth range from 220 km to the CMB. This biased volumetric model was inferred from S rays that bottom in the lower mantle and that were imprinted with travel time perturbations from the models Topo410b and Topo660b. The upper-mantle r.m.s. bias of the Chebyshev-based volumetric model is about 10% to about 20% of the r.m.s. of S12_WM13, and decreases monotonically with depth. The r.m.s. bias of the shell-based inversion is apparently larger, but taking into account the oscillation (or change in sign) across the 410 km discontinuity, the integrated bias of the two parametrizations is similar. Nearly all of the biased volumetric structure, for both radial parametrizations, is in or directly above the transition zone. This result can be understood by referring to Fig. 3(a) (bottom), which displays the paths of rays that bottom in the lower mantle. Rays that cross the transition zone boundaries close to one another (less than 2000 km apart) have similar travel time signals. However, they may bottom in entirely different regions of the lower mantle ranging from just beneath the transition zone to just above the CMB. Similarly, rays which cross the transition zone boundaries at entirely different (lateral) locations may bottom at the same location in the lower mantle. For the lower-mantle bottoming rays, the best-fitting volumetric structure has most of its r.m.s. amplitude in the upper mantle where the rays are steep and experience nearly identical travel time perturbations. Lower-mantle bottoming rays are efficient at mapping structure into the uppermost regions of the mantle volume, but they are not able to separate the topographic signals from the two boundaries. In regions where there are crossing rays that are nearly horizontal, there is little bias.

Quite different results are obtained when rays that bottom in the transition zone are included. Fig. 6(b) shows the r.m.s. of the shear velocity perturbation relative to S12_WM13 that results from the combined inversion of lower-mantle and transition zone bottoming rays. The average r.m.s. bias ranges from 2% to 4% in the transition zone, depending on the parametrization used. However, with this data set, the r.m.s. amplitude maximizes in the regions directly above and directly below the transition zone, rather than in radial intervals centered about the boundaries. The av-

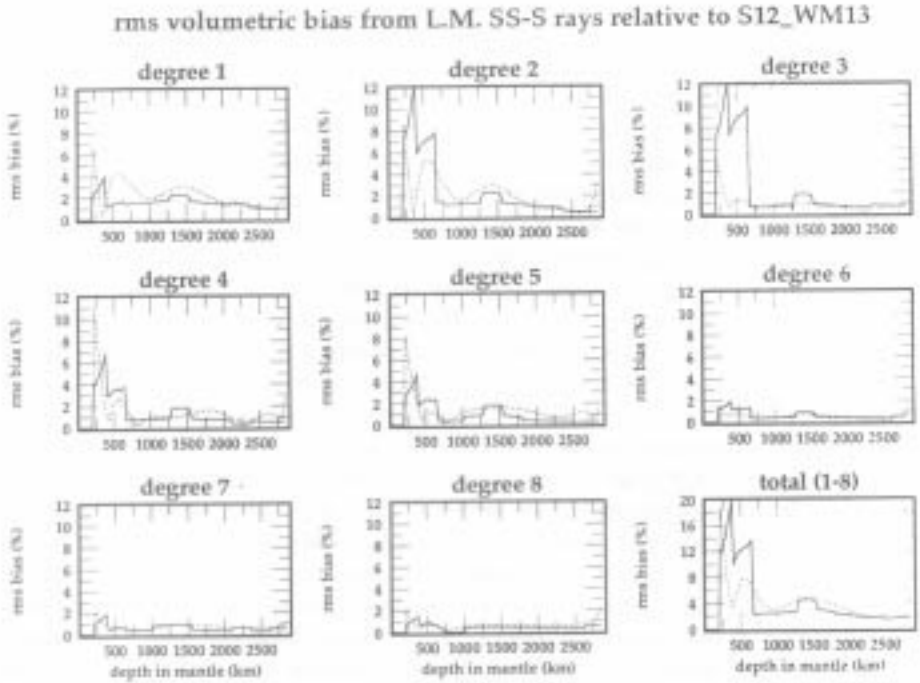

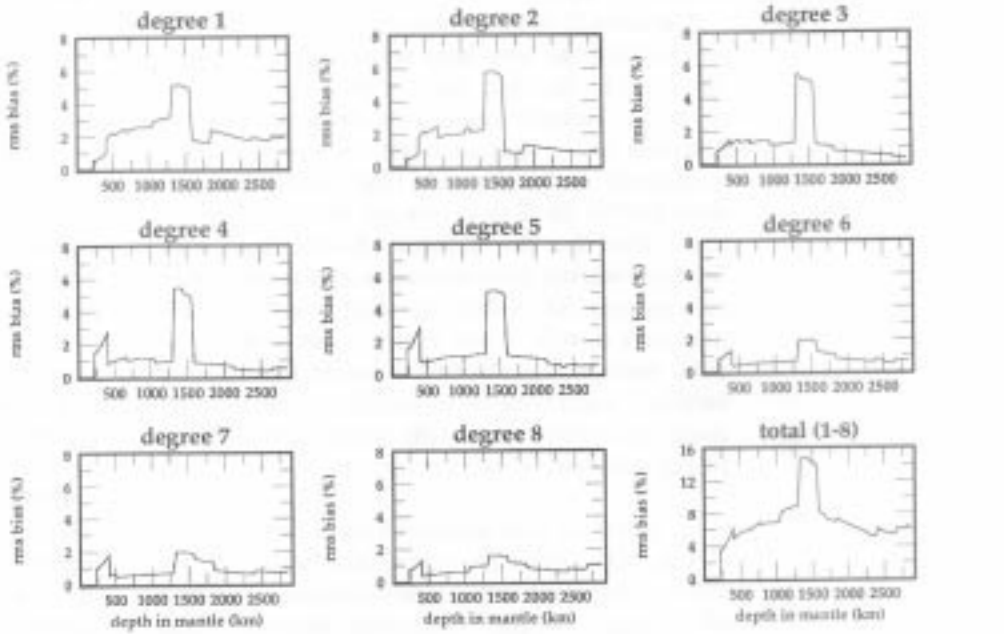

Fig. 7. (a) Similar to Fig. 6(a), but for SS–S phase pairs with the SS legs bottoming in the lower mantle only. (b) Similar to Fig. 6(a), but for SS–S phase pairs with the SS legs bottoming in both the transition zone and the lower mantle.

erage bias near the top of the lower mantle is about 10%, and is about 5% in the high gradient zone. In essence, the Topo410b signal is mapped into the region above the transition zone and the Topo660b signal is mapped into the region directly below the transition zone. The inclusion of rays that bottom in the transition zone constrains the structure in that region and also separates the topographic signals from the 410 and 660 km discontinuities. The use of transition zone bottoming S waves in the inversion reduces the average transition zone r.m.s. bias by a factor of about three relative to the inversion of the first S ray data set, and acts to redistribute the biased structure from the transition zone dominantly into the lower mantle.

In general, two characteristics of body wave travel time data sets are necessary for inferences of volumetric structure to be reliable. First, rays used in the inversion must possess uniform azimuthal sampling; i.e. they must cross one another. We avoid problems associated with insufficient azimuthal sampling by using rays with a uniform geographical sampling. Second, inversions for structure in a given radial interval must include rays that bottom throughout the interval. As the absolute S waves that bottom in the lower mantle and transition zone are imprinted with similar travel time perturbations from topography on the transition zone boundaries, but sample entirely different regions away from the boundaries, models with significant structure in the lower mantle cannot simultaneously fit upper-mantle and lower-mantle bottoming rays. This is why the r.m.s. amplitude of biased volumetric structure in the mid- and lowermost mantle for both inversion experiments is strongly diminished. Rays with epicentral distances less than 17° were not included in the inversion experiments and, thus, there were no rays that bottomed above 400 km depth. The large r.m.s. value of the bias near the top and bottom of the mantle model parametrized with Chebyshev polynomials is a feature shared with the normal mode–mantle wave inversions.

3.2.2. Inversion with differential SS–S travel times

The result of the SS–S inversion experiment for the data set in which the SS legs bottom in the lower mantle only is displayed in Fig. 7(a). The r.m.s. amplitude of the biased volumetric structure is largest in the depth range from 220 to 660 km, and is diminished in the lower mantle, much like the biased structure inverted from S waves that bottom in the lower mantle alone. The undamped solutions allow one oscillation across the 410 km boundary. Taking this into account, the average amplitude of the bias in the upper

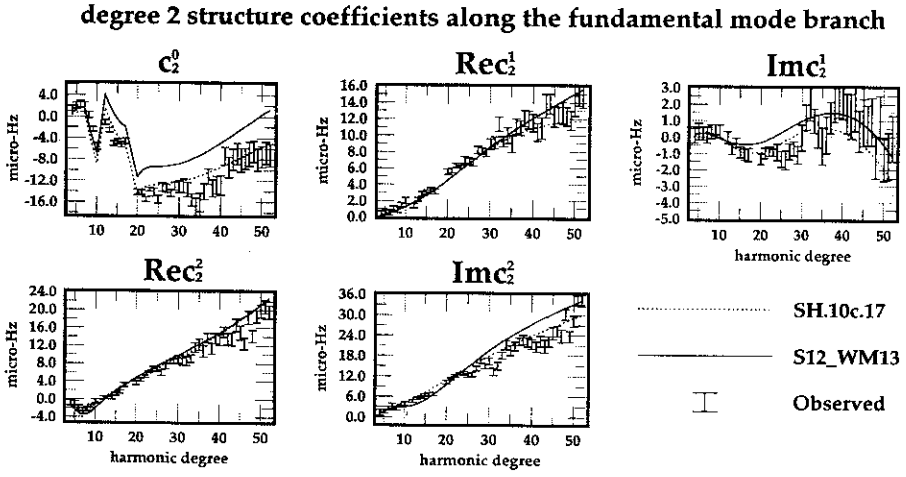

Fig. 8. Predicted and observed Degree 2 structure coefficients (Eq. (4)) for S12_WM13 (solid line), and SH.10c.17 (dotted line). The data were taken from Smith and Masters (1989a).

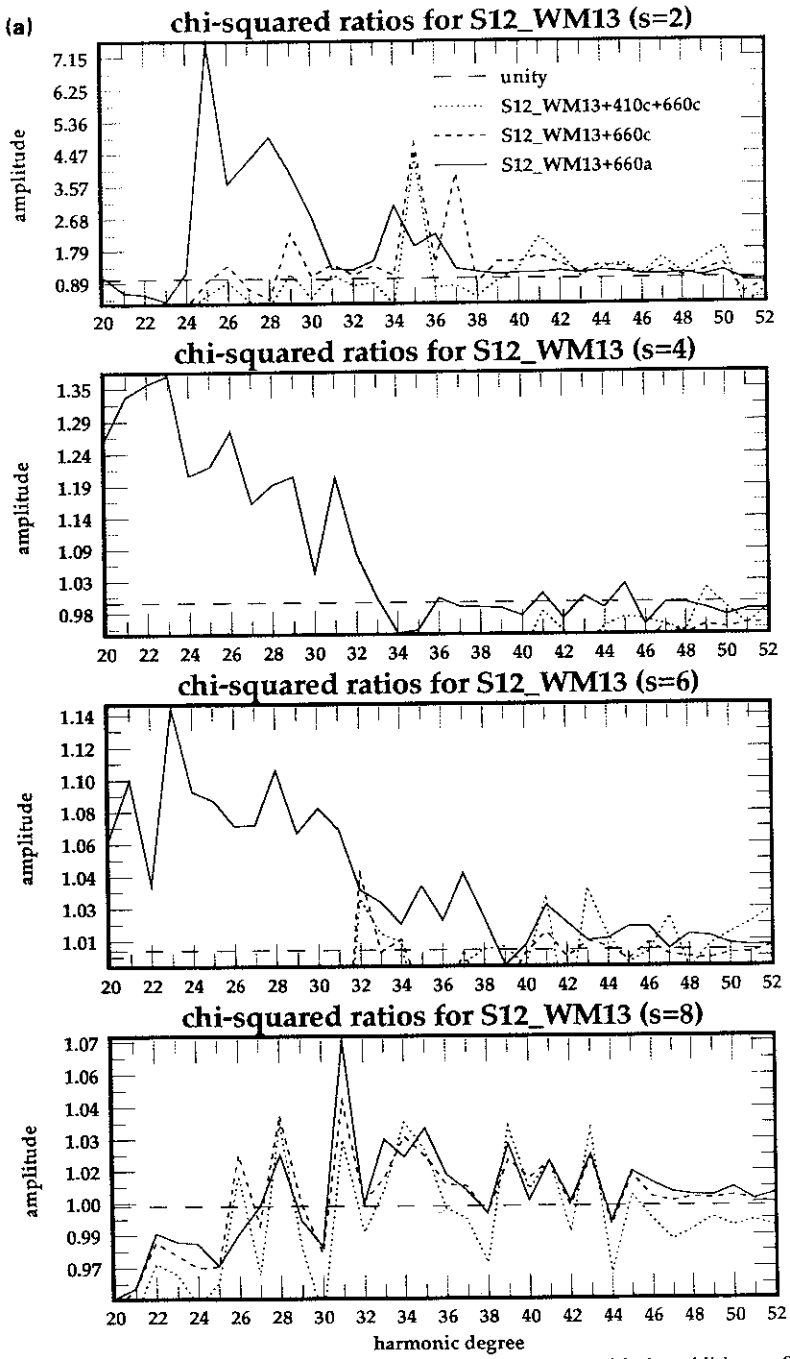

Fig. 9. (a) Misfit improvement (or degradation) to the observed structure coefficients with the addition to S12_WM13 of Topo660a (solid line), Topo660c (dashed line), and Topo410c + Topo660c (dotted line) for modes along the fundamental branch in the range $20 \leqslant l \leqslant 52$. Panels 1–4 correspond, respectively, to even degrees of structure 2–8. Improved fits to the data are reflected by χ^2 ratios greater than unity (above the long-dash line). The χ^2 ratios approach unity as the boundary sensitivity decreases. Only those ratios that fall within the range defined by the minimum and maximum values of the solid line are shown. (b) Misfit improvement (or degradation) to the observed structure coefficients with the addition to SH.10c.17 of Topo660a (solid line), Topo660b (dashed line), and Topo410b + Topo660b (dotted line). Otherwise, the same as (a).

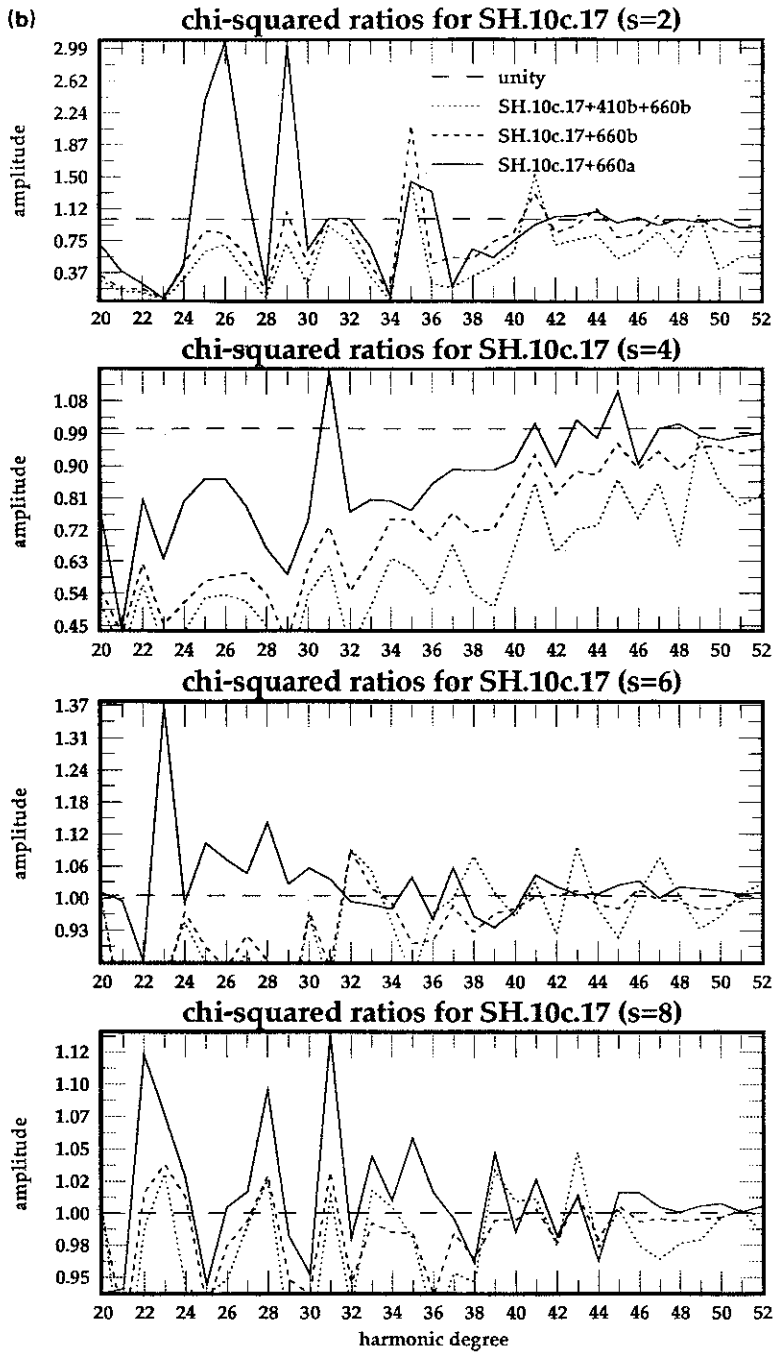

Fig. 9 (continued).

mantle is about 8% relative to S12_WM13. The fact that the r.m.s. amplitude is greatest in the upper mantle can be understood as follows. SS crosses the transition zone boundaries at four points. The differential travel time signal incurred by S and SS rays that penetrate the

boundaries at the two points near to the source and receiver is very small because the topography is nearly identical at these crossing points. The SS rays that cross the 410 and 660 km boundaries twice near the surface bounce point of SS accumulate a travel time signature of topographic structure there which is not offset by a similar signature in S. This dominates the differential travel time signature. Consequently, these travel time signals are mapped into the regions near the 410 and 660 km discontinuity crossing points in the region approximately beneath the SS bounce points. The r.m.s. amplitude in the lower mantle is small relative to that in the upper mantle for two reasons: (1) the SS rays are nearly insensitive to structure in the lower mantle as they do not bottom at depths greater than 1200 km; (2) S rays bottoming in the lower mantle from different azimuths contain topographic signals from entirely different lateral locations; thus, these signals destructively interfere and produce a small r.m.s. amplitude of bias. The average transition zone r.m.s. amplitude of the bias inverted from this SS–S data set is reduced by a factor of about two relative to the r.m.s. bias of the normal mode–mantle wave inversion in the transition zone.

Fig. 7(b) displays the result of the inversion of the SS–S data set containing SS legs that bottom in and below the transition zone, and results are displayed for the shell-based parametrization only. The average r.m.s. bias across the upper mantle is about 5% relative to S12_WM13. The bias is comparable with that displayed in Fig. 6(a) for the inversion experiment that used absolute S rays that bottomed in and below the transition zone.

3.3. Joint inversion of normal mode–mantle wave and body wave data

If normal mode–mantle wave and body wave data were inverted simultaneously, the resultant volumetric bias would be a function of the weighting of the individual data sets and the correlation of the biased structures from the individual data sets. As the correlations tend to be high, the results would depend mostly on the data weighting used. This introduces another free parameter into the inversion, and is the reason we do not pursue joint inversions further here.

4. Combining volumetric and topographic models

In this section we examine the relationship between the boundary models of Shearer and Masters (1992) and Shearer (1993) with current volumetric models. The question we seek to address, and which will be discussed further in Section 5.1, is the following: has the trade-off between volumetric and topographic structure been resolved by current volumetric models? The approach adopted here is to determine if the addition of the global topographic models to the volumetric models improves the fit to observed normal mode–mantle wave structure coefficients. This approach is useful as long-period mantle waves display significant sensitivity to boundary undulations on the 410 and 660 km boundaries (Fig. 2). In Section 4.1, we discuss the computation of the predicted structure coefficients. We adopt χ^2 statistics as the measure of misfit between model predictions and data, and present in Section 4.2 functions of these statistics for various combinations of topographic and volumetric models to address the question posed above.

4.1. Observed and predicted structure coefficients

Fig. 8 displays the Degree 2 structure coefficients observed by Smith and Masters (1989a) for multiplets along the fundamental mode branch, as well as the predicted coefficients of the volumetric models S12_WM13 (solid line) and SH.10c.17 (dotted line). The predicted coefficients were computed using Eq. (4), and were made comparable with the observed coefficients by including crustal and Coriolis coupling corrections (Smith and Masters, 1989b). Crustal corrections were applied to the predicted coefficients of S12_WM13 and SH.10c.17 using, respectively, the Harvard crustal model (Woodhouse and Dziewonski, 1984) and the Scripps crustal model (Smith and Masters, 1989a). These corrections have been discussed in greater detail by Ritz-

woller and Lavely (1994b). The crustal model of Su et al. (1994) extends the Harvard crustal model to Degree 12, but the models are identical to Degree 8.

In the following, the fit of the predicted to the observed c_2^0 coefficients will be ignored as the predicted values vary substantially between the two models. The accuracy of the Coriolis coupling correction to these coefficients is strongly dependent on an accurate spherical reference model. In addition, there exists a substantial discrepancy between the Scripps and Harvard crustal models in the predicted values of the crustal correction for axisymmetric Degree 2 structure. It is impractical to display the observed and predicted structure coefficients for all of the relevant volumetric and topographic model combinations. However, the fit of these model combinations to the data are displayed in terms of functions of χ^2 statistics in the following section.

4.2. χ^2 statistics and data misfit

In this section χ^2 statistics are used to compare the observed normal mode structure coefficients with the structure coefficients computed for various combinations of the 410 and 660 km topographic models with the volumetric models S12_WM13 and SH.10c.17. In the present context, interpretation of χ^2 statistics is meaningful only if computed for the range of multiplets that display significant sensitivity to the appropriate boundaries. For example, Fig. 2 shows that 660 km boundary models have the most significant effect on fundamental modes above the Coriolis coupling regime in the range $20 \leqslant l \leqslant 35$, and that 410 km boundary models are important for fundamental modes in the range $30 \leqslant l \leqslant 52$. The inclusion of multiplets in a χ^2 summation that are outside the domains of influence would tend to obscure the effect of boundary models on data misfit statistics. Thus, we consider individual multiplets separately and sum over all azimuthal orders for each degree of structure.

Of relevance here is whether the addition of a given topographic model to a given volumetric model enhances or degrades the data misfit. Thus, we introduce the χ^2 ratio statistic $\chi^2_{ratio}(s, k)$ which is defined as the ratio of χ^2 values computed using a given volumetric model and a combined volumetric + topographic model for the kth multiplet and degree s of structure:

$$\chi^2_{\text{ratio}}(s, k) = \frac{\chi^2_{s,k}(\text{volumes})}{\chi^2_{s,k}(\text{volumes} + \text{topography})} = \frac{\sum_{t=-s}^{s} \left(\frac{{}_k\tilde{c}_s^t - {}_kc_s^t}{{}_k\sigma_s^t} \right)^2}{\sum_{t=-s}^{s} \left(\frac{{}_k\tilde{c}_s^t + {}_k\hat{c}_s^t - {}_kc_s^t}{{}_k\sigma_s^t} \right)^2} \quad (7)$$

where ${}_kc_s^t$ is the observed structure coefficient for the kth multiplet, ${}_k\tilde{c}_s^t$ is the sum of the predicted mantle-volumetric, crustal, and Coriolis coupling structure coefficients, ${}_k\hat{c}_s^t$ is the predicted topographic structure coefficient, and ${}_k\sigma_s^t$ is the uncertainty estimated for ${}_kc_s^t$. We call the statistic defined in Eq. (7) the χ^2 ratio.

Values of the χ^2 ratio greater than unity signify that the addition of a topographic model to the volumetric model improves the fit to the data, and ratios less than unity reflect a degradation in fit to the data. Values of this statistic for the volumetric model S12_WM13 relative to the model combinations S12_WM13 + Topo660a (solid line), S12_WM13 + Topo660c (dashed line), and S12_WM13 + Topo410c + Topo660c (dotted line) are shown in Fig. 9(a) for even degrees $2 \leqslant s \leqslant 8$. In analogy to Fig. 9(a), Fig. 9(b) displays the χ^2 ratios for the volumetric model SH.10c.17 relative to the model combinations SH.10c.17 + Topo660a (solid line), SH.10c.17 + Topo660b (dashed line), and SH.10c.17 + Topo410b + Topo660b (dotted line).

Figs. 9(a) and 9(b) are usefully viewed in conjunction with Fig. 2, which displays the sensitivity of fundamental modes to a unit perturbation on the 410 and 660 km boundaries. The addition of Topo660a to S12_WM13 appears to improve the fit to the Degree 2 coefficients for the majority of the multiplets in the range considered. In particular, the ratios are maximized in the range of maximum modal sensitivity to structure on the 660 km boundary. In contrast, the model combinations Topo660c + S12_WM13 and Topo410c +

Topo660c + S12_WM13 are characterized by χ^2 ratios that on average are below unity. Thus, the addition of these topographic models to S12_WM13 degrades the fit to the structure coefficients relative to the fit achieved using S12_WM13 alone.

The addition of Topo660a to SH.10c.17 improves the fit to the observed coefficients for only a few of the multiplets. The combined models Topo410b + Topo660b + SH.10c.17 and Topo660b + SH.10c.17 degrade the fit for almost all of the multiplets at all degrees of structure. In general, the fit of SH.10c.17 to the observed coefficients is more strongly degraded by the addition of the class b topographic models than S12_WM13 is degraded by the addition of the class c topographic models. It is not surprising that the addition of topographic models to SH.10c.17 generally does not improve the fit to the data as the even-degree components of SH.10c.17 have been designed to fit the structure coefficients with purely volumetric structure. The Degree 8 topographic corrections are small relative to the errors of the observed coefficients and, thus, the χ^2 ratios approach unity for all model combinations. The interpretation of these results is discussed further in Section 5.1.

5. Discussion

In this section we discuss the implications of the inversion experiments described in Section 3 and the misfit statistics reported in Section 4. In Section 3 it was shown how normal mode–mantle wave and body wave inversions for volumetric structure can be biased by unmodeled topographic structure. In Section 4 it was shown that topographic boundary models when added to volumetric models can significantly affect the fit to observed normal mode structure coefficients. These findings immediately suggest two questions: have current models of mantle-volumetric structure resolved the trade-off between volumetric structure and topography on the 410 and 660 km boundaries? If not, does there exist a combination of normal mode and body wave travel time data that can be used to resolve the trade-off? These questions are discussed, respectively, in Sections 5.1 and 5.2.

5.1. Has the trade-off between volumetric and topographic structure been resolved?

To address if the trade-off between volumetric and topographic structures has been resolved by current models of 3D volumetric structure in the mantle, we investigate if the combination of the global topographic models with current volumetric models improves the fit to observed normal mode structure coefficients. The combination of an accurate boundary model with a volumetric model that has resolved the trade-off should provide a better fit to observed normal mode structure coefficients than the volumetric model alone.

The χ^2 ratios displayed in Fig. 9(a) demonstrate that the combined model Topo660a + S12_WM13 significantly improves the fit to observed normal mode structure coefficients relative to the fit achieved with the volumetric model S12_WM13 alone. Any other topographic model is incompatible with all of the volumetric models because, as Figs. 9(a) and 9(b) show, the combination of the boundary models Topo410b, Topo410c, Topo660b, and Topo660c with the volumetric models S12_WM13 and SH.10c.17 generally degrades the fit to the observed structure coefficients relative to the fit achieved using the volumetric models alone.

The observation that the model combination S12_WM13 + Topo660a satisfies our consistency test is intriguing, but does not necessarily imply that S12_WM13 has resolved the trade-off between volumetric and topographic structure. One problem is that the structure coefficients observed to date constrain only the even-degree components of boundary and volumetric structures. Thus, the fit to the odd-degree components cannot be assessed. A more serious problem is that this approach is only a consistency test, and is not conclusive as the boundary model Topo660a may not be accurate. In fact, Topo660a apparently was constructed using an erroneous surface topographic correction, and has been subsequently disavowed by Shearer (1993). In addition, the class b and c models are intimately coupled

with the reference volumetric and crustal models used to remove the effects of volumetric heterogeneity.

The use of the method employed here to test if volumetric models have resolved the volumetric–topographic trade-off will only be conclusive when the boundary models are believed to represent accurate global models. The first-generation global topographic models are probably fairly accurate in certain well-sampled regions, but are less reliable as global models. As the reference volumetric models continue to improve, and the global sampling of SS–SdS phase pairs becomes more uniform with the addition of data from new networks, the reliability of the global-scale features of later-generation topographic models will improve as well.

In addition to testing the consistency between the seismic volumetric and topographic models, there are a number of other geophysical data with which the consistency of the global boundary models of Shearer and Masters (1992) and Shearer (1993) can be determined. For example, regional high-resolution studies of 660 km topography (e.g. Wicks and Richards, 1993) can be compared with the Topo660a, b, and c boundary models. Another approach is that of Morgan and Shearer (1993), in which the observed topography is used to infer the requisite density heterogeneity that deforms the boundary. The density heterogeneity inferred using this procedure can then be compared with the heterogeneity implied by global seismic models and slab models (subject to suitable scaling relationships). In addition, predicted and observed geoid coefficients, and geodynamically computed flow patterns can be compared with observations.

5.2. *Can the trade-off between volumetric and topographic structure be resolved?*

There are two ways, in principle, to resolve the trade-off between volumetric and topographic structures. The first method is to use waves that do not sample a specific boundary but do constrain the volume directly above the boundary. If a body wave ray path or a mantle wave–normal mode sensitivity kernel does not intersect a boundary, then the associated datum will be insensitive to that boundary. Thus, body waves that turn or a normal mode whose exponential tail is directly above a boundary are able to constrain the volume above the boundary with reduced contamination from topography on the boundary directly below. In this way the addition of turning S waves or SS waves in the transition zone in the synthetic experiments described in Section 3.2 reduced the bias in this region. The problem with this method is that data of the requisite sort have been relatively few in number and they resolve the trade-off only for the volumes above a boundary. Consequently, bias tends to decrease above the boundary but increases below it. This is not particularly bad news for the transition zone, as the bias in this region caused by topography on the 410 km boundary is not very large, but is bad news for attempts to calibrate the top of the lower mantle. Another problem is that body waves have a Fresnel zone of non-negligible width. Thus, body waves that turn above a boundary may nonetheless be influenced by the boundary.

The second method is based on the observation that the efficiency of biasing is inversely proportional to the radial resolving power of the data. Radial S-wave resolution lengths are short in comparison with normal modes–mantle waves and for SS–S phase pairs in which there is large radial separation between the bottoming points of the S and SS phases. Consequently, absolute S-wave travel time measurements cannot be fitted as efficiently with the radially coarse volumetric basis functions that define global models as can the normal mode–mantle wave structure coefficients and the differential travel times, and the r.m.s. amplitudes of the resultant biased models are reduced. The problem with the use of absolute S-wave travel times is that they are sensitive to contamination owing to near-source structures, which diminishes their capacity to resolve the trade-off.

As the efficiency of biasing is dependent on the radial resolving power of the data, an estimate of the radial resolution of current 3D models would be useful. The resolving power can be characterized through the use of the radial correlation function $R(r, r')$ introduced by Jordan et

al. (1993). This function defines the geographical correlation of aspherical structure on the spherical surfaces r and r'. The variation in this function with radius identifies the characteristic scales of radial change within a model. $R(r, r')$ defines a 2D function whose value is unity on the diagonal ($r = r'$), and whose decay away from the diagonal characterizes the rate of decorrelation of structures on spherical surfaces as their radii separate. Fig. 10 is a plot of $R(r, r')$ for the volumetric model SH.10c.17. The odd degrees of this model are constrained by body wave data including S waves and SS–S phase pairs. The radial correlation function shows that the resolving power of the pure body wave data set is poorer than that of the combined body wave and normal mode–mantle wave data set that constrain the even degrees of this model.

To make progress in resolving the topographic–volumetric bias, the first of the methods described above is the more likely alternative. Therefore, the best hope for desensitizing the transition zone structure to bias caused by topography on the boundaries that surround it is to fit preferentially SS–S differential travel times for SS waves that bottom in the transition zone ($25° < \Delta < 40°$) and to fit mantle wave data sensitive to the transition zone but insensitive to the 660 km boundary. As Fig. 11 illustrates, the relevant mantle waves will lie approximately in the interval between ${}_0S_{45}$ and ${}_0S_{80}$.

Current global models are incorporating ex-

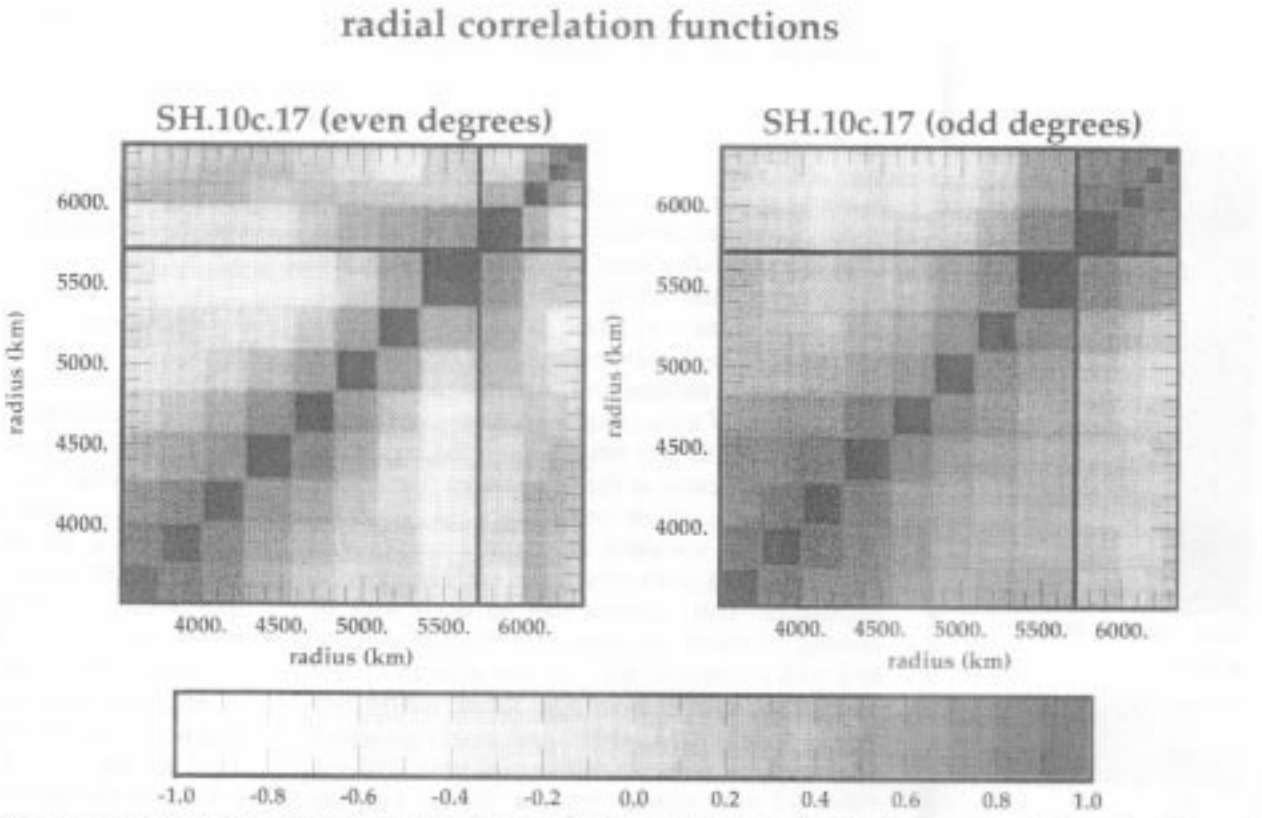

Fig. 10. Even-degree (left) and odd-degree (right) radial correlation functions for SH.10c.17. The correlation lengths of the odd-degree component of the model are greater than the correlation lengths of the even component. As the odd components of this model are not constrained by normal mode data, this suggests that the body waves used in the construction of SH.10c.17 (dominantly SS–S) have lower resolving power than the normal modes and body waves that constrained the even-degree part of the model.

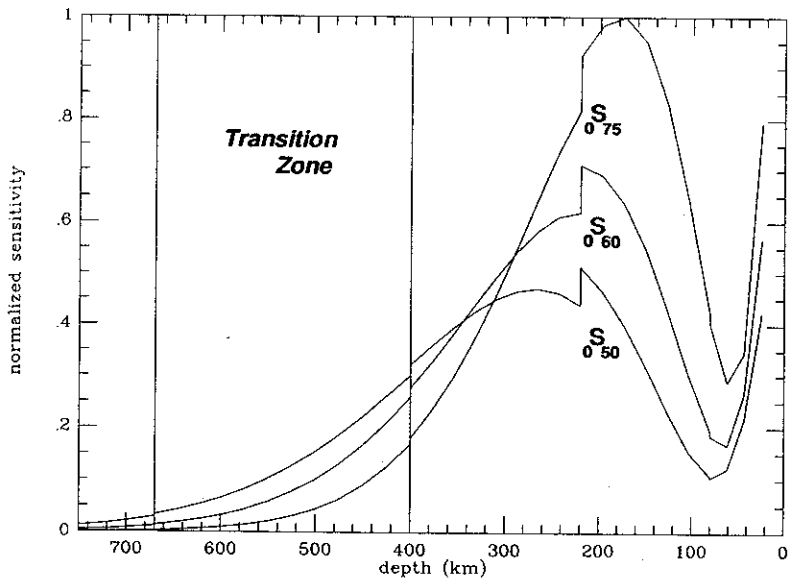

Fig. 11. Sensitivity kernels for three fundamental multiplets across the upper mantle, demonstrating differential sensitivity to the transition zone with only low sensitivity to topography on the 660 km boundary.

pansions in the data used, both in type and frequency, and are currently moving in the directions recommended here. However, most of the SS–S differential travel time measurements to date have been for phase pairs with SS legs bottoming in the lower mantle. This is due to the distribution of sources and receivers, and due to the difficulty of measuring the differential time of pairs with the SS legs bottoming in the transition zone. SS triplicates at the top and bottom of the transition zone, which complicates the SS waveform, making standard differential travel time estimates using cross-correlation with observed S impossible. This problem can be dealt with by making SS travel time estimates through correlation with a synthetic trace as was done by Grand and Helmberger (1985), who fitted WKBJ synthetics both to the direct and to the bounced phases to estimate the differential time. The addition of new seismic stations in the last few years, especially in Asia in regions near large topographic depressions in the 660 km boundary models of Shearer and Masters (1992) and Shearer (1993), should allow the observation of many more relevant SS phases and the calibration of the transition zone models in this region.

6. Conclusions

The purpose of this paper has been to address three questions for which we briefly summarize the conclusions here.

(1) To what extent does unmodeled structure on the 410 and 660 km boundaries bias volumetric structure in inversions based on normal mode–mantle wave structure coefficients, absolute S-wave travel times, and differential SS–S travel times? We have shown that inversions for volumetric structure based on normal mode–mantle wave data can be biased by realistic topographic structures on the 410 and 660 km boundaries at the 20% level in the transition zone relative to the volumetric model S12_WM13. The bias peaks in the vicinity of the boundaries. Inversion experiments based on absolute S-wave travel times with S waves that bottom in and below the transition zone, or on SS–S phase pairs that

include SS legs that bottom in and below the transition zone yield biased volumetric models with transition zone r.m.s. amplitudes reduced by a factor of about three to five relative to the r.m.s. bias of models inverted from normal modes–mantle waves. Inversions based on SS–S phase pairs that include only SS legs yield bottoming in the lower mantle biased transition zone r.m.s. amplitudes reduced by a factor of about two to three relative to the normal modes–mantle waves biased model.

(2) Can the differences in the sensitivity of S waves, differential phase pairs such as SS–S, and normal mode data be exploited to estimate transition zone volumetric models that are relatively unbiased by topographic structure? In principle, the fundamentally different sensitivity kernels of absolute S waves compared with normal modes or SS–S phase pairs can be used to overcome partially the trade-off between volumetric and topographic structures. In practice, the use of absolute S travel times to resolve the trade-off is complicated by the difficulty of removing signal contamination from near-source structure. The contamination owing to near-source structure can be mitigated by the use of differential phase pairs such as SS–S, but unless the inversion includes SS legs that bottom in the transition zone, the use of phase pairs sacrifices the radial resolution that is needed to resolve the trade-off between volumetric and topographic structures.

(3) Have current volumetric models resolved the trade-off that exists between volumetric and topographic structures? The combined model Topo660a + S12_WM13 represents the sole combined boundary and volumetric model that improved the fit to normal mode structure coefficients relative to the volumetric model alone. This suggests that S12_WM13 may have resolved the trade-off, but this result is equivocal as Topo660a has been disavowed by Shearer (1993). The addition of the class b and c topographic models of Shearer (1993) to the reference volumetric models degrades the fit to the normal mode structure coefficients. However, we only can infer from this that the volumetric models have not resolved the trade-off between volumetric and topographic structure if the more recent topographic models are themselves relatively error free.

Acknowledgments

We would like to thank John Wahr for many valuable discussions. We thank Wei-jia Su for sending a manuscript before publication and for supplying the model coefficients of S12_WM13, Guy Masters for providing the coefficients of SH.10c.17, and Harold Bolton for providing the coefficients of the Scripps crustal model. We thank Peter Shearer for sending a manuscript before publication. We would also like to thank the editors, Hanneke Paulssen and Gilles Bussod, for their guidance and assistance, and for putting together this special transition zone issue. E.M.L. was supported by a Ford Foundation Postdoctoral Fellowship and a CIRES Visiting Fellowship.

References

Benz, H.M. and Vidale, J.E., 1993. Sharpness of upper-mantle discontinuities determined from high-frequency reflections. Nature, 365: 147–150.

Creager, K.C. and Jordan, T.H., 1986. Aspherical structure of the core–mantle boundary from PKP travel times. Geophys. Res. Lett., 13: 1497–1500.

Dehant, V. and Wahr, J., 1991. The response of a compressible, nonhomogeneous earth to internal loading: theory. J. Geomagn. Geoelectr., 43: 157–175.

Dziewonski, A.M., 1984. Mapping the lower mantle: determination of lateral heterogeneity in P velocity up to degree and order 6. J. Geophys. Res., 89: 5929–5952.

Dziewonski, A.M. and Anderson, D.L., 1981. Preliminary Reference Earth Model. Phys. Earth Planet. Inter., 25: 297–356.

Dziewonski, A.M. and Gilbert, F., 1976. The effect of small aspherical perturbations on travel times and a re-examination of the corrections for ellipticity. Geophys. J.R. Astron. Soc., 44: 7–17.

Dziewonski, A.M., Forte, A.M., Su, W.-J. and Woodward, R.L., 1993. Seismic tomography and geodynamics. In: K. Aki and R. Dmowska (Editors), Proceedings of the Jeffreys Symposium. Geophys. Monogr. 76. Am. Geophys. Union, Washington, DC, pp. 67–105.

Edmonds, A.R. 1960. Angular Momentum in Quantum Mechanics. Princeton University Press, Princeton, NJ.

Forte, A.M. and Peltier, R., 1991. Viscous flow models of global geophysical observables: 1. Forward problems. J. Geophys. Res., 96: 20131–20159.

Forte, A.M. and Peltier, W.R., 1991. Core–mantle boundary topography and whole-mantle convection. Geophys. Res. Lett., 16: 621–624.

Forte, A.M, Dziewonski, A.M. and Woodward, R.L., 1993. Aspherical structure of the mantle, tectonic plate motions, nonhydrostatic geoid, and topography of the core–mantle boundary. In: Dynamics of Earth's Deep Interior and Earth Rotation. Geophys. Monogr. 72. IUGG Vol. 12. Am. Geophys. Union, Washington, DC, pp. 135–136.

Giardini, D., Li, X.-D. and Woodhouse, J.H., 1988. The splitting functions of long period normal modes of the Earth. J. Geophys. Res., 93: 13716–13742.

Grand, S.P. and Helmberger, D.V., 1985. Upper mantle shear structure beneath Asia from multi-bounce S waves. Phys. Earth Planet. Inter., 41: 154–169.

Gudmunsson, O., Clayton, R.W. and Anderson, D.L., 1986. CMB topography inferred from ISC PcP travel times. EOS, Trans. Am. Geophys. Union, 67: 1100.

Hager, B.H., 1984. Subducted slabs and the geoid: constraints on mantle rheology and flow. J. Geophys. Res., 89: 6003–6015.

Hager, B.H. and Clayton, R.W., 1989. Constraints on the structure of mantle convection using seismic observations, flow models, and the geoid. In: W.R. Peltier (Editor), Mantle Convection. Gordon and Breach, New York, pp. 657–763.

Hager, B.H. and Richards, M.A., 1989. Long-wavelength variations in the Earth's geoid: physical models and dynamical implications. Philos. Trans. R. Soc. London, Ser. A, 328: 309–327.

Hager, B.H., Clayton, R.W., Richards, M.A., Comer, R.P. and Dziewonski, A.M., 1985. Lower mantle heterogeneity, dynamic topography, and the geoid. Nature, 313: 541–545.

Inoue, H., Fukao, Y., Tanabe, K. and Ogata, Y., 1990. Whole mantle P-wave travel time tomography. Phys. Earth Planet. Inter., 59: 294–328.

Jordan, T.H., Puster, P., Glatzmaier, G.A. and Tackley, P.J., 1993. Comparisons between seismic Earth structures and mantle flow models based on radial correlation functions. Science, 261: 1427–1431.

Li, X.-D., Giardini, D. and Woodhouse, J.H., 1991. Large-scale three-dimensional even-degree structure of the Earth from splitting of long-period normal modes. J. Geophys. Res., 91: 551–577.

Masters, G., Bolton, H. and Shearer, P., 1992. Large-scale 3-dimensional structure of the mantle. EOS, Trans. Am. Geophys. Union, 73: 201.

Montagner, J.-P. and Tanimoto, T., 1990. Global anisotropy in the upper mantle inferred from the regionalization of phase velocities. J. Geophys. Res., 95: 4797–4819.

Montagner, J.-P. and Tanimoto, T., 1991. Global upper mantle tomography of seismic velocities and anisotropies. J. Geophys. Res., 96: 20337–20351.

Morelli, A. and Dziewonski, A.M., 1987. Topography of the core–mantle boundary and lateral homogeneity of the liquid core. Nature, 325: 678–683.

Morgan, J.P. and Shearer, P.M., 1993. Seismic constraints on mantle flow and topography of the 660-km discontinuity: evidence for whole-mantle convection. Nature, 365: 506–511.

Neele, F. and Snieder, R., 1992. Topography of the 400 km discontinuity from observations of long-period $P_{400}P$ phases. Geophys. J. Int., 109: 670–682.

Nishimura, C. and Forsyth, D., 1989. The anisotropic structure of the upper mantle in the Pacific. Geophys. J.R. Astron. Soc., 96: 203–229.

Olson, P., Silver, P.G. and Carlson, R.W., 1990. The large-scale structure of convection in the Earth's mantle. Nature, 344: 209–215.

Park, J., 1987. Asymptotic coupled-mode expressions for multiplet amplitude anomalies and frequency shifts on an aspherical earth. Geophys. J.R. Astron. Soc., 90: 129–169.

Paulssen, H., 1988. Evidence for a sharp 670-km discontinuity as inferred from P-to-S converted waves. J. Geophys. Res., 93: 10489–10500.

Pulliam, R.J., Vasco, D.W. and Johnson, L.R., 1993. Tomographic inversions for mantle P-wave velocity structure based on the minimization of l^2 and l^1 norms of ISC travel time residuals. J. Geophys. Res., 98: 699–734.

Revenaugh, J. and Jordan, T.H., 1989. A study of mantle layering beneath the western Pacific. J. Geophys. Res., 94: 5787–5813.

Revenaugh, J. and Jordan, T.H., 1991a. Mantle layering from ScS reverberations: 2. The transition zone. J. Geophys. Res., 96: 19763–19780.

Revenaugh, J. and Jordan, T.H., 1991b. Mantle layering from ScS reverberations: 3. The upper mantle. J. Geophys. Res., 96: 19781–19780.

Richards, M.A. and Wicks, Jr., C.W., 1990. S–P conversion from the Transition Zone beneath Tonga and the nature of the "650-km" discontinuity. Geophys. J. Int., 101: 1.

Ritzwoller, M.H. and Lavely, E.M., 1994a. Long period surface waves and mantle boundary undulations. Geophys. J. Int., 116: 204.

Ritzwoller, M.H. and Lavely, E.M., 1994b. Three-dimensional seismic models of the Earth's mantle. Rev. Geophys., in press.

Ritzwoller, M.H., Masters, G. and Gilbert, F., 1988. Constraining aspherical structure with low harmonic degree interaction coefficients: application to uncoupled multiplets. J. Geophys. Res., 93: 6269–6396.

Rodgers, A. and Wahr, J., 1993. Inference of core–mantle boundary topography from ISCPcP and PKP travel times. Geophys. J. Int., 115: 991–1011.

Rodgers, A. and Wahr, J., 1994. The trade-off between volumetric and topographic structure for seismic travel times: 660-km topography and mantle structure. Geophys. J. Int., 117: 19–32.

Romanowicz, B.A., 1991. Seismic tomography of the Earth's Mantle. Annu. Rev. Earth Planet. Sci., 19: 77–79.

Roult, G., Romanowicz, B. and Montagner, J.P., 1990. 3D

upper mantle shear velocity and attenuation from fundamental mode free oscillation data. Geophys. J.R. Astron. Soc., 101: 61–80.

Shearer, P.M., 1990. Seismic imaging of upper-mantle structure with new evidence for a 520-km discontinuity. Nature, 344(6262): 121–126.

Shearer, P.M., 1991a. Constraints on upper mantle discontinuities from observations of long-period reflected and converted phases. J. Geophys. Res., 96: 18147–18182.

Shearer, P.M., 1991b. Imaging global body wave phases by stacking long-period seismograms. J. Geophys. Res., 96: 20353–20364.

Shearer, P.M., 1993. Global mapping of upper mantle reflectors from long-period SS precursors. Geophys. J. Int., 115: 878–904.

Shearer, P.M. and Masters, T.G., 1992. Global mapping of topography on the 660-km discontinuity. Nature, 355: 791–796.

Smith, M.F. and Masters, G., 1989a. Aspherical structure constraints from free oscillation frequency and attenuation measurements. J. Geophys. Res., 94: 1953–1976.

Smith, M.F. and Masters, G., 1989b. The effect of Coriolis coupling of free oscillation multiplets on the determination of aspherical earth structure. Geophys. Res. Lett., 16: 263–266.

Su, W.-J., Woodward, R.L. and Dziewonski, A.M., 1994. Degree-12 model of shear velocity heterogeneity in the mantle. J. Geophys. Res., 99: 6945–6980.

Tanimoto, T., 1990. Long-wavelength S-wave velocity structure throughout the mantle. Geophys. J. Int., 100: 327–336.

Vidale, J.E. and Benz, H.M., 1992. Upper mantle seismic discontinuities and the thermal structure of subduction zones. Nature, 356: 678–682.

Wicks, Jr., C.W. and Richards, M.A., 1993. A detailed map of the 660-km discontinuity beneath the Izu–Bonin subduction zone. Science, 261: 1424–1427.

Woodhouse, J.H., 1980. The coupling and attenuation of nearly resonant multiplets in the earth's free oscillation spectrum. Geophys. J.R. Astron. Soc., 61: 261–283.

Woodhouse, J.H. and Dahlen, F.A., 1978. The effect of a general aspherical perturbation on the free oscillations of the Earth. Geophys. J.R. Astron. Soc., 53: 335–354.

Woodhouse, J.H. and Dziewonski, A.M., 1984. Mapping the upper mantle: three dimensional modelling of Earth structure by inversion of seismic waveforms. J. Geophys. Res., 89: 5953–5986.

Woodward, R.L. and Masters, G., 1991a. Upper mantle structure from long-period differential travel times and free oscillation data. Geophys. J. Int., 109: 275–293.

Woodward, R.L. and Masters, G., 1991b. Lower-mantle structure from ScS–S differential travel times. Nature, 352: 231–233.

Woodward, R.L., Forte, A.M., Su, W.-J. and Dziewonski, A.M., 1993. Evolution of the earth and Planets. Geophys. Monogr. 74. Am. Geophys. Union, Washington, DC, pp. 89–109.

Zhang, Y.-S. and Tanimoto, T., 1993. High-resolution global upper mantle structure and plate tectonics. J. Geophys. Res., 98: 9793–9823.

Note to contributors

The Editors invite colleagues who are preparing papers within the scope of the Journal to submit them for publication. Please note that the manuscripts should be written in the English language. A detailed *Guide for Authors* is available on request, and is also printed in Vol. 82, No. 1, pp. 83–86. You are kindly requested to consult this guide.

Letter Section

The *Letter Section* is entirely devoted to short manuscripts describing preliminary results, suggestions for new applications of analytical methods, new theories, etc.

Communications intended for this PEPI Letter Section should not exceed six printed pages and should be self-contained. The manuscripts received will be published *not later than three months* after their final acceptance.

Manuscripts should contain a brief summary of approx. 50 words. In order to achieve rapid publication, no proofs will be sent to the authors. Manuscripts should therefore be prepared with the greatest possible care.

Preparation of the text

(a) The manuscript should be typewritten with double spacing and wide margins and include, at the beginning of the paper, an abstract of not more than 500 words. Words to be printed in italics should be underlined. The S.I. unit system should be used throughout.
(b) The title page should include: the title, the name(s) of the author(s) and their affiliations, in that order.

References

(a) References in the text start with the name of the author(s), followed by the publication date in parentheses.
(b) The reference list should be in alphabetical order and on sheets separate from the text, in the following style:

Bullen, K.E., 1975. The Earth's Density. Chapman and Hall, London, 420 pp.
Kanamori, H. and Cipar, J.J., 1974. Focal processes of the great Chilean earthquake May 22, 1960. Phys. Earth Planet. Inter., 9: 128–136.
Knopoff, L., 1972. Model for the aftershock occurrence. In: H.C. Heard, I.Y. Borg, N.L. Carter and C.B. Raleigh (Editors), Flow and Fracture of Rocks. Am. Geophys. Union, Geophys. Monogr. Ser., 16: 259–263.
Toksöz, M.N., Thomson, K.C. and Ahrens, T.J., 1971. Generation of seismic waves in prestressed media. Bull. Seismol. Soc. Am., 61: 1589–1623.

Names of journals should be abbreviated according to the *Bibliographic Guide for Editors*, published by the American Chemical Society, Washington, DC, USA.

Tables

Tables should be compiled on separate sheets. A title should be provided for each table and they should be referred to in the text.

Illustrations

(a) All illustrations should be numbered consecutively and referred to in the text.
(b) Drawings should be completely lettered, the size of the lettering being appropriate to that of the drawings, but taking into account the possible need for reduction in size (preferably not more than 50%). The page format of the Journal should be considered in designing the drawings.
(c) Photographs must be of good quality, printed on glossy paper.
(d) Figure captions should be supplied on a separate sheet.

Proofs

One set of proofs will be sent to the author, to be carefully checked for printer's errors (the Publisher does not read proofs). In the case of two or more authors please indicate to whom the proofs should be sent.

Page charges and reprints

There will be *no page charge*. Each author receives with his proofs a reprint order form which must be completed and returned to the Publisher with the proofs. *Fifty reprints* of each article are supplied *free of charge*.

Submission of manuscript

Manuscripts should be submitted in triplicate to one of the three Editors, whose addresses are listed on the front inside cover. Illustrations should also be submitted in triplicate. One set should be in a form ready for reproduction; the other two may be of lower quality.

Submission of electronic text

In order to publish the paper as quickly as possible after acceptance authors are encouraged to submit the final text also on a 3.5" or 5.25" diskette. Both double density (DD) and high density (HD) diskettes are acceptable. However, the diskettes should be formatted according to their capacity (HD or DD) before copying the files onto them. Similar to the requirements for manuscripts submission, main text, list of references, tables and figure legends should be stored in separate text files with clearly identifiable file names. The format of these files depends on the wordprocessor used. Texts made with DisplayWrite, MultiMate, Microsoft Word, Samna Word, Sprint, TeX, Volkswriter, Wang PC, WordMARC, WordPerfect, Wordstar, or supplied in DCA/RFT, or DEC/DX format can be readily processed. In all other cases the preferred format is DOS text or ASCII. It is essential that the name and version of the wordprocessing program, type of computer on which the text was prepared, and format of the text files are clearly indicated. The final manuscript may contain parts (e.g. formulae, complex tables) or last minute corrections which are not included in the electronic text on the diskette; however, these should be clearly marked on an additional hardcopy of the manuscript.

Books for review should be addressed to: Editorial Office Earth Sciences, Elsevier Science B.V., P.O. Box 1930, 1000 BX Amsterdam.

Submission of an article is understood to imply that the article is original and unpublished and is not being considered for publication elsewhere.

Upon acceptance of an article by the journal, the author(s) resident in the USA will be asked to transfer the copyright of the article to the Publisher. This transfer will ensure the widest possible dissemination of information under the US Copyright Law.

0031-9201/94/$07.00